Endothelial p53 Deletion Improves Angiogenesis and Prevents Cardiac Fibrosis and Heart Failure Induced by Pressure Overload in Mice

Rajinikanth Gogiraju, PhD; Xingbo Xu, PhD; Magdalena L. Bochenek, PhD; Julia H. Steinbrecher, MSc; Stephan E. Lehnart, MD; Philip Wenzel, MD; Michael Kessel, PhD; Elisabeth M. Zeisberg, MD; Matthias Dobbelstein, MD; Katrin Schäfer, MD

Background—Cardiac dysfunction developing in response to chronic pressure overload is associated with apoptotic cell death and myocardial vessel rarefaction. We examined whether deletion of tumor suppressor p53 in endothelial cells may prevent the transition from cardiac hypertrophy to heart failure.

Methods and Results—Mice with endothelial-specific deletion of p53 (End.p53-KO) were generated by crossing p53$_{fl/fl}$ mice with mice expressing Cre recombinase under control of an inducible Tie2 promoter. Cardiac hypertrophy was induced by transverse aortic constriction. Serial echocardiography measurements revealed improved cardiac function in End.p53-KO mice that also exhibited better survival. Cardiac hypertrophy was associated with increased p53 levels in End.p53-WT controls, whereas banded hearts of End.p53-KO mice exhibited lower numbers of apoptotic endothelial and non-endothelial cells and altered mRNA levels of genes regulating cell cycle progression (p21), apoptosis (Puma), or proliferation (Pcna). A higher cardiac capillary density and improved myocardial perfusion was observed, and pharmacological inhibition or genetic deletion of p53 also promoted endothelial sprouting in vitro and new vessel formation following hindlimb ischemia in vivo. Hearts of End.p53-KO mice exhibited markedly less fibrosis compared with End.p53-WT controls, and lower mRNA levels of p53-regulated genes involved in extracellular matrix production and turnover (eg, Bmp-7, Ctgf, or Pai-1), or of transcription factors involved in controlling mesenchymal differentiation were observed.

Conclusions—Our analyses reveal that accumulation of p53 in endothelial cells contributes to blood vessel rarefaction and fibrosis during chronic cardiac pressure overload and suggest that endothelial cells may be a therapeutic target for preserving cardiac function during hypertrophy. (*J Am Heart Assoc.* 2015;00:e001770 doi: 10.1161/JAHA.115.001770)

Key Words: angiogenesis • endothelium • fibrosis • heart failure • p53

Cardiac hypertrophy develops as adaptive response of the heart to chronically increased afterload, such as elevated blood pressure or aortic stenosis, but may progress to ventricular dilation and cardiac dysfunction, if continued over the long term. Clinical and experimental evidence suggests that the rarefaction of cardiac capillaries observed in chronic cardiac hypertrophy promotes tissue hypoxia, cell death, and replacement fibrosis and contributes to the progression from compensated hypertrophy to contractile dysfunction and heart failure.[1–3] A central role of cardiac endothelial cells and angiogenesis is supported by findings that inhibition of new blood vessel formation accelerates the development of left ventricular (LV) dysfunction,[4,5] whereas stimulation of angiogenesis improves cardiac function and delays the onset of heart failure.[6–8] However, the molecular mechanisms involved in the regulation of cardiac angiogenesis and in particular, the reduction of cardiac vessel density during pathological hypertrophy are incompletely understood.

Elevated levels of tumor suppressor p53 have been reported in myocardial biopsies of patients with heart disease[9] and found to progressively increase with disease severity.[10] Increased apoptotic cell numbers have also been described in rodents following transverse aortic constriction (TAC),[11] a model frequently used to study the cellular and

molecular changes during cardiac hypertrophy and failure.[12] Experimental studies could show that global p53 deficiency protects against cardiac injury,[13,14] and that p53 activation accelerates LV function deterioration,[15] supporting a causal role of apoptotic cell death and p53 in the development of heart failure. In addition to its role as master regulator of cellular senescence, cell cycle arrest and apoptosis, p53 is involved in the transcriptional regulation of genes controlling diverse biological processes, such as differentiation, migration, or angiogenesis.[16] However, and although a considerable number of endothelial cells also undergoes apoptotic cell death after TAC,[17] the role of endothelial p53 expression for the cardiac response to chronic pressure overload is largely unknown.

In this study, we examined whether deletion of the tumor suppressor p53 in endothelial cells is able to preserve the cardiac microvasculature, to prevent pathological cardiac remodeling and the development of fibrosis in response to chronic pressure overload and to postpone the transition from cardiac hypertrophy to heart failure.

Methods

Experimental Animals

To generate mice with inducible endothelial cell–specific p53 deletion (End.p53-KO), mice with loxP-flanked (floxed, fl) p53 alleles (C57BL/6 background; courtesy of Anton Berns)[18] were mated with mice expressing a Cre recombinase-estrogen receptor fusion protein ER(T2) under control of the endothelial receptor tyrosine kinase (Tie2) promoter (C57BL/6 background; courtesy of Berndt Arnold).[19] This inducible Tie2.Cre mouse line has been shown to allow efficient temporal gene deletion exclusively in endothelial cells, including the heart, whereas the percentage of recombined cells was found to be negligible in hematopoietic cells.[19] Cre recombinase activity was induced by feeding 5- to 6-week-old mice with rodent chow containing 400 mg/kg tamoxifen citrate (TD55125; Harlan Teklad) for 6 weeks.[19] Cre-WT x p53fl/fl mice fed tamoxifen chow were used as controls (End.p53-WT). Age- and gender-matched littermates were used throughout the study. All animal care and experimental procedures were in accordance with institutional guidelines and had been approved by the institutional Animal Research Committee and the Lower Saxony State Office for Consumer Protection and Food Safety and complied with national guidelines for the care and use of laboratory animals.

Determination of Blood Pressure

Systolic and diastolic blood pressure was obtained in awake mice using a tail cuff noninvasive blood pressure system (CODA Monitor; Kent Scientific Corporation). A minimum of three measurements was obtained from each mouse.

Vascular Function Studies

The thoracic part of aortas isolated from End.p53-WT and End.p53-KO mice was liberated from perivascular adipose tissue, cut into 4 mm-sized pieces and carefully rinsed to completely remove any blood from inside the vessel. The endothelium-intact segments were put on force transducers (Kent Scientific Corporation) in organ chambers filled with Krebs–Henseleit solution to perform concentration-contraction and -relaxation curves in response to increasing concentrations of phenylephrine, acetylcholine (ACh), or glyceryl trinitrate (GTN), as described previously.[20]

Transverse Aortic Constriction

Female mice were anesthetized via 2% isoflurane inhalation and subjected to minimally invasive TAC surgery over a 26-gauge needle.[21] Anesthesia depth was monitored by observing the respiratory rate and the toe-pinch reflex. Sham-operated mice, in which the aortic arch was exposed, but not ligated, were also examined. Three days after surgery, the pressure gradient over the aortic ligature was determined using pulsed wave Doppler. At tissue harvest, hearts were rapidly excised and weighed. Atria were removed and ventricles immediately processed for RNA and protein isolation, cryoembedding, or endothelial cell isolation.

Echocardiography

Two-dimensional (2D) echocardiography was performed by a blinded observer in mice under 1.5% isoflurane anesthesia using the Vevo 2100 system (Visualsonics) equipped with a 30 MHz center frequency ultrasound transducer.[21] On average, heart rate was 460±15 bpm, respiratory rate was 125±3.8 breaths/min. M-mode recordings were used to determine the end-diastolic (EDD) and end-systolic (ESD) LV chamber diameter and the anterior (AWTh) and posterior wall thickness (PWTh). Echocardiographic LV weight was estimated using the formula: $1.055 \times ([AWTh+EDD+PWTh]^3 - EDD^3)$. Fractional shortening (FS) was calculated as $(EDD-ESD)/EDD \times 100$.

Unilateral Hindlimb Ischemia

Neovascularization in vivo was examined using the unilateral hindlimb ischemia mouse model in male mice.[22] Perfusion was determined before and the indicated time points after surgery via laser Doppler perfusion imaging (LDPI; PeriScan PIM III, Perimed) using the contralateral hindlimb as internal control (set at 100%).

Histochemistry

Histochemical analyses were performed on frozen, acetone-fixed cross sections through the LV of mice 8 and 20 weeks after TAC or sham operation or the lower hindlimb of mice 4 weeks after femoral artery ligation, respectively. Cardiac fibrosis was determined by Masson's trichrome (MTC) staining. Interstitial collagen was visualized using picrosirius red staining. Capillary endothelial cells were assessed using monoclonal antibodies against CD31 (Santa Cruz Biotechnology), followed by Cy3-labeled secondary antibodies (Molecular Probes). The functionality of cardiac vessels was determined by intracardiac (i.c.) injection of endothelial fluorescein isothiocyanate (FITC)-conjugated Griffonia simplicifolia isolectin B4 (50 μg in 200 μL saline; Vector Laboratories) 15 minutes prior to sacrifice. Cells not positive following CD31 antibody incubation or endothelial lectin perfusion are denoted as "CD31-negative cells" or "lectin-negative cells," respectively. Endothelial function was examined using rabbit polyclonal antibodies against eNOS (Abcam), VCAM-1 (Abcam), and caveolin-1 (Cell Signaling Technology). Cardiomyocyte membranes were visualized using FITC-labeled wheat germ agglutinin (WGA; Molecular Probes) followed by determination of the single cardiomyocyte cross-sectional area (CSA). Per cross section, 10 randomly selected cardiomyocytes were evaluated and results averaged. Cardiac apoptosis was examined using TUNEL (Roche) and antibodies against activated caspase-3 (Promega) or p53 (Cell Signaling Technology).

A rabbit anti-carbonic anhydrase IX (CAIX) antibody (Bioss Antibodies) was used as surrogate marker for hypoxia.[23] Fibroblast-specific protein (FSP)-1 was detected using a polyclonal rabbit anti-mouse antibody (Dako Cytomation). All morphometric analyses were performed using image analysis software (Image ProPlus, version 4.01).

Quantitative Real Time PCR

Total RNA was isolated using TRI Reagent (Ambion), and the amount and quality checked by spectrophotometry (Nanodrop; Thermo Scientific). One μg RNA was reversed transcribed into cDNA, followed by quantitative PCR using *real-time* assessment of SYBR Green (Applied Biosystems) and the iCycler iQ Detection system (BioRad). Primers and qPCR conditions are listed in Table. All qPCR data (two or more biological replicates with three technical replicates each) were calculated using the delta delta Ct method and normalized to Gapdh RNA, and are reported as -fold change versus sham-operated mice (set at 1).

Western Blot Analysis

Frozen heart tissue was pulverized in liquid nitrogen and resuspended in lysis buffer containing fresh protease and phosphatase inhibitors. Equal amounts of protein were fractionated by SDS polyacrylamide gel electrophoresis

Table. Primer Sequences and qRT-PCR Conditions

Gene	Primer Sequence (in 5′→3′ Direction)	T_m (°C)	Cycles	Reference
Bmp7	F: ACCCTTCATGGTGGCCTTCT R: CCTCAGGGCCTCTTGGTTCT	58	40	47
Col1a1	F: ATGGATTCCCGTTCGAGTACG R: TCAGCTGGATAGCGACATCG	60	35	40
Ctgf	F: CTTCTGCGATTTCGGCTCC R: TACACCGACCCACCGAAGA	60	35	48
Gapdh	F: GCACAGTCAAGGCCGAGAAT R: GCCTTCTCCATGGTGGTGAA	57	40	49
Mmp2	F: ACCCAGATGTGGCCAACTAC R: TACTTTTAAGGCCCGAGCAA	57	40	50
Mmp9	F: GAGCTGTGCGTCTTCCCCTTC R: GGAATGATCTAAGCCCAGTGC	58	40	51
p21	F: CCTGACAGATTTCTATCACTCCA R: GCAGGCAGCGTATATCAGGAG	60	40	51
p53	F: CACAGCGTGGTGGTACCTTA R: TCTTCTGTACGGCGGTCTCT	60	40	52
Pai-1	F: TCGTGGAACTGCCCTACCAG R: ATGTTGGTGAGGGCGGAGAG	60	35	48
Pcna	F: TTGGAATCCCAGAACAGGAG R: CAGTGGAGTGGCTTTTGTGA	57	40	53
Puma	F: ATGGCGGACGACCTCAAC R: AGTCCCATGAAGAGATTGTACATGAC	60	40	*
Slug	F: CGCTCCTTCCTGGTCAAGA R: AGGTATAGGGTAACTTTCATAGAGATA	60	40	*
αSma	F: CCACCGCAAATGCTTCTAAGT R: GGCAGGAATGATTTGGAAAGG	58	40	54
Snail	F: GTGCCCACCTCCAAACCC R: AAGGACATGCGGGAGAAGG	60	40	*
Tgfβ	F: CAGTGGCTGAACCAAGGAGAC R: ATCCCGTTGATTTCCACGTG	60	35	48
Twist	F: TGATAGAAGTCTGAACACTCGTTTG R: GGCTGATTGGCAAGACCTCT	60	40	*
Vimentin	F: CGGAAAGTGGAATCCTTGCA R: CACATCGATCTGGACATGCTGT	60	40	55

PCR indicates polymerase chain reaction; TGFβ, transforming growth factor-beta.

*Primer sequences were designed and purchased from Primerdesign Ltd. (Southampton, UK).

together with molecular weight standards and transferred to nitrocellulose membranes (Protran; Whatman). Membranes were blocked in 5% BSA or nonfat dry milk (in TBS buffer containing 0.1% Tween-20), followed by incubation with antibodies against p53 (Cell Signaling Technology), Hif1α (Abcam), or Vegf (Millipore). Protein bands were visualized using horseradish peroxidase-conjugated secondary antibodies (Amersham Biosciences), followed by detection with SuperSignal West Pico Substrate (Pierce). Protein bands were quantified by densitometry and normalized to Gapdh (HyTest Ltd) or β-actin (Millipore) protein, and are expressed as -fold change versus sham-operated mice (set at 1).

Cardiac Endothelial Cell Isolation

To isolate cardiac CD31-positive and -negative cells, mice were sacrificed and their hearts excised and diced into 1 mm-sized pieces. Fragments were incubated in enzyme digestion buffer (1X PBS with 0.1% dextrose, containing 5 mg/mL collagenase type II and 60 U/mL deoxyribonuclease DNAse II) under continuous shaking at 37°C. Dulbecco's Modified Eagle's Medium (DMEM) containing 10% FBS was used to stop the reaction. After a brief centrifugation, the cell pellet was resuspended, passed through a 40 μm mesh filter and a second digestion performed for 30 seconds. Cells were subsequently surface labeled using CD31-phycoerythrin-conjugated antibodies (Biolegend) and sorted using the FACSaria II cell sorter (BD).

Cell Culture Studies

Human Cardiac Microvascular Endothelial Cells (HCMECs; PromoCell) were cultured at 37°C under 5% CO_2 in Endothelial Cell Growth Medium (EGM; PromoCell). Pifithrin-α and nutlin-3a were purchased from Sigma-Aldrich. Human p53 shRNA expression vectors or scrambled non-effective shRNA cassette (in pGFP-C-shLenti plasmid) were obtained from Amsbio. A lentivirus-based TP53 human shRNA (OriGene) construct was used to generate a stable p53 knockdown endothelial cell line. For EndMT induction, HCMECs were incubated with TGFβ$_1$ (R&D Systems; 10 ng/mL for 6 or 12 days); to induce chemical hypoxia, HMCECs were treated with cobald chloride ($CoCl_2$; 1 mmol/L for 4 h).

Angiogenesis Assay

To study angiogenic cell functions, 3.2×10^4 HCMECs were resuspended in 10 mL EGM containing 20% methylcellulose and analyzed using the spheroid angiogenesis assay.[22] Pictures of 10 spheroids at random phase contrast microscopy fields were taken and analyzed by image analysis software (Image ProPlus).

Statistical Analysis

Quantitative data are presented as mean±SEM. Normal distribution was confirmed for all data sets using the D'Agostino & Pearson omnibus normality test. Differences between two groups were tested by Student t test for unpaired means. If more than two groups were compared, ANOVA test (or repeated measures ANOVA, if findings in the same animal before and after an intervention were compared) was performed followed by Bonferroni's Multiple Comparison test. Frequencies were compared using the χ^2 test. Survival analysis was performed using the log-rank test. Statistical significance was assumed if P reached a value less than 0.05. All analyses were performed using data analysis software (version 6.0; GraphPad Software Inc).

Results

To generate endothelial-specific p53 KO mice (End.p53-KO), mice carrying floxed p53 alleles[18] were crossed with mice expressing Cre recombinase under control of an inducible Tie2 promoter (Tie2.ERT.Cre), previously shown to allow efficient temporal gene deletion exclusively in endothelial cells, including the heart, whereas the percentage of recombined cells was found to be negligible in hematopoietic cells.[19] Successful p53 gene excision was confirmed by PCR analysis of genomic DNA from tail biopsies (Figure 1A). Quantitative *real-time* PCR analysis confirmed significantly reduced p53 mRNA levels in CD31-positive cells isolated from hearts of End.p53-KO mice compared with CD31-positive cells isolated from End.p53-WT mice or CD31-negative cells (Figure 1B). Of note, endothelial cell-specific p53 deletion *per se* did not affect survival up to 12 months and was not associated with spontaneous tumor formation (not shown).

Endothelial p53 Deletion Does Not Lead to Endothelial Dysfunction Under Basal Conditions

Immunostaining of cross sections through the uninjured aorta revealed marked and similar expression of caveolin-1 and eNOS in both genotypes, whereas endothelial p53 or VCAM1 were not detected (Figure 2A). Vascular contraction and relaxation studies of aortic rings revealed no differences between both genotypes in their response to phenylephrine (Figure 2B), the endothelium-dependent vasodilator acetylcholine (Figure 2C), or to glyceryl trinitrate (Figure 2D). Systemic blood pressure also was similar (ie, 126±12 mm Hg in End.p53-WT and 127±14 in End.p53-KO mice; n=11 mice per group). These findings suggested that lack of p53 in endothelial cells does not result in endothelial dysfunction under basal conditions.
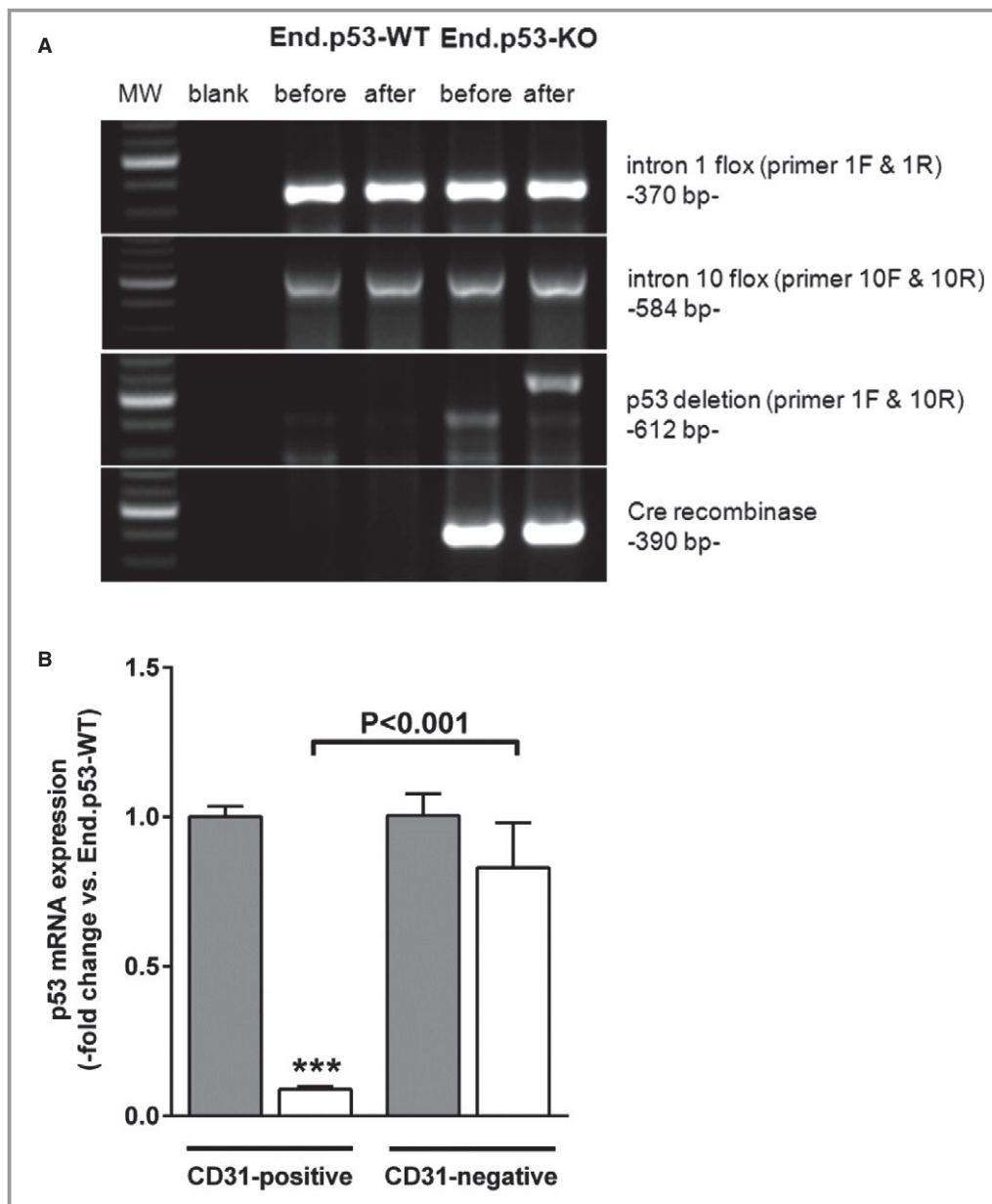
Figure 1. Genotyping of endothelial p53 knockout and wildtype mice. A, Genomic DNA was isolated from mouse tail biopsies obtained before and 6 weeks after feeding mice tamoxifen citrate–containing chow and amplified by PCR. Floxed p53 alleles were identified using forward (F) and reverse (R) primer against intron 1 or intron 10. Excision of p53 exons was confirmed in Cre recombinase transgenic mice. B, qPCR analysis of p53 mRNA expression in CD31-positive and CD31-negative cells, isolated from hearts of End.p53-WT (grey bars; n=6) and End.p53-KO (white bars; n=6) mice. ***$P<0.001$ vs CD31-positive cells isolated from End.p53-WT mice. Significant differences between CD31-positive and CD31-negative cells of End.p53-KO mice are indicated within the graph. MW indicates molecular weight marker; PCR, polymerase chain reaction.

Endothelial p53 Deletion Protects From Cardiac Dysfunction After Pressure Overload

To induce cardiac hypertrophy, female mice were subjected to TAC surgery. Mean pressure gradients over the aortic valve were similar in both groups, ie, 71 ± 3.8 mm Hg in End.p53-KO and 74 ± 3.7 mm Hg in End.p53-WT mice

(P=0.51). As shown in Figure 3A, survival (after exclusion of mice that died within the first 24 h after surgery) was improved in End.p53-KO mice (5 out of 34 mice died) compared with their End.p53-WT counterparts (16 out of 41 mice died; P=0.020). Serial echocardiographic measurements revealed a marked decline in cardiac function in End.p53-WT mice, beginning at week 4 after TAC and
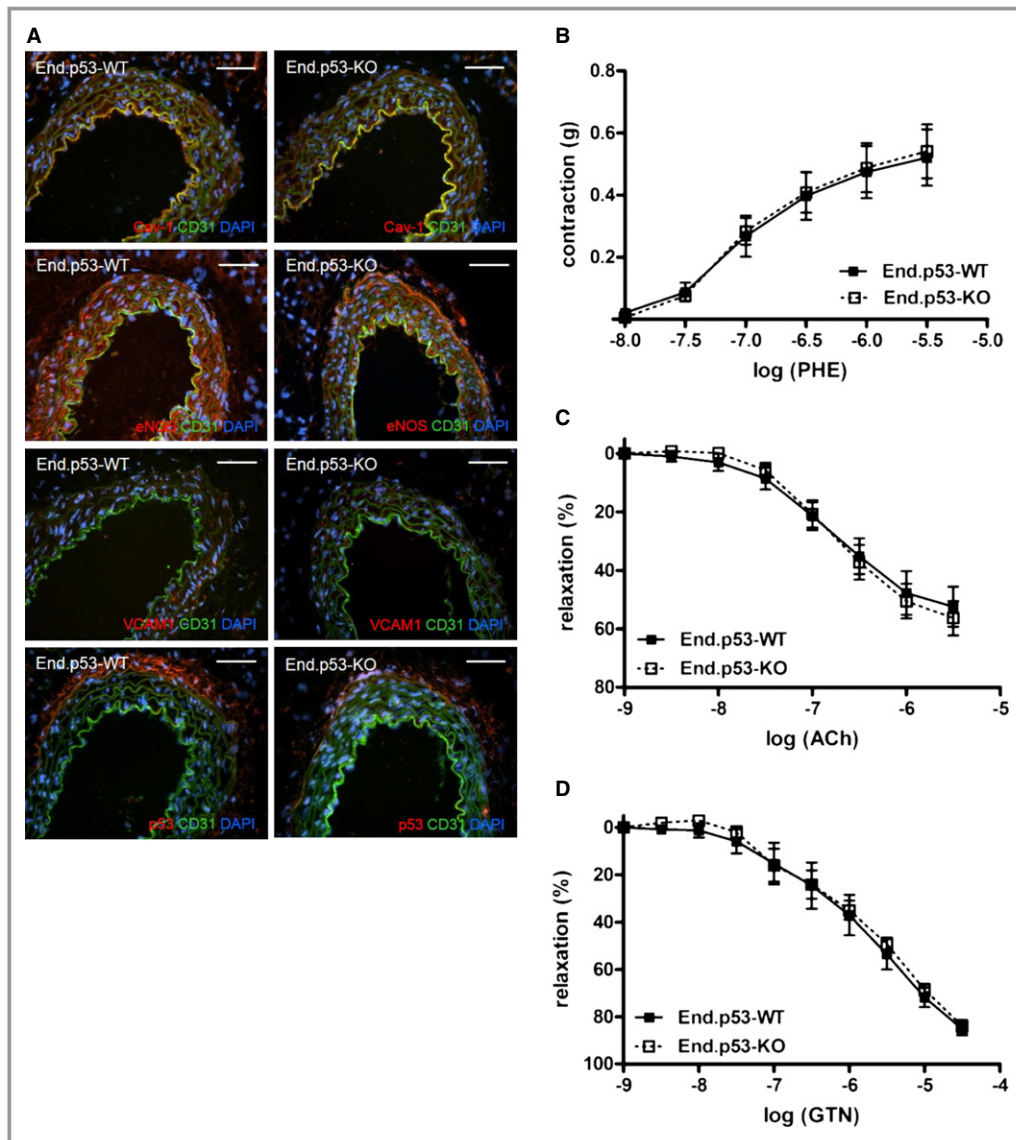
Figure 2. Vascular function analysis in endothelial p53 wildtype and knockout mice. A, Representative fluorescence images after immunostaining for caveolin-1 (Cav-1), eNOS, VCAM-1 or p53 in the aorta of End.p53-WT and End.p53-KO mice. CD31 was used to identify endothelial cells, DAPI to visualize cell nuclei. Size bars represent 100 μm. B through D, Contraction and relaxation curves of isolated rings of thoracic aortas from End.p53-WT (n=8) or End.p53-KO (n=6) mice in response to increasing concentrations of phenylephrine (B), acetylcholine (Ach; C) or glyceryl trinitrate (GTN; D). DAPI indicates 4′,6-diamidino-2-phenylindole.

progressing towards week 20 (Figure 3B). The reduction of fractional shortening (FS) was significantly less pronounced in End.p53-KO mice compared with End.p53-WT mice at 8 and 20 weeks after TAC. Compared with baseline, a significant increase in the endsystolic (not shown) and enddiastolic (Figure 3C) LV inner diameter was observed in both genotypes, which progressed further only in End.p53-WT mice and was significantly more pronounced compared with End.p53-KO mice 20 weeks after TAC. At this time point, the mean PWTh (*P*<0.05; Figure 3D) and echocardiographically determined LV weight (*P*<0.05; Figure 3E) were

significantly increased in End.p53-WT compared to End.p53-KO mice, and this observation was confirmed by determining the actual heart weight at necropsy (Figure 3F). On the histological level, the mean single cardiomyocyte cross-sectional area (CSA) was significantly increased after TAC in both genotypes, although to a lesser extent in End.p53-KO mice (*P*<0.05 versus End.p53-WT at 20 week after TAC; Figure 4), suggesting that inducible deletion of p53 in endothelial cells ameliorates the development of cardiac hypertrophy and attenuates the deterioration of cardiac function after pressure overload.
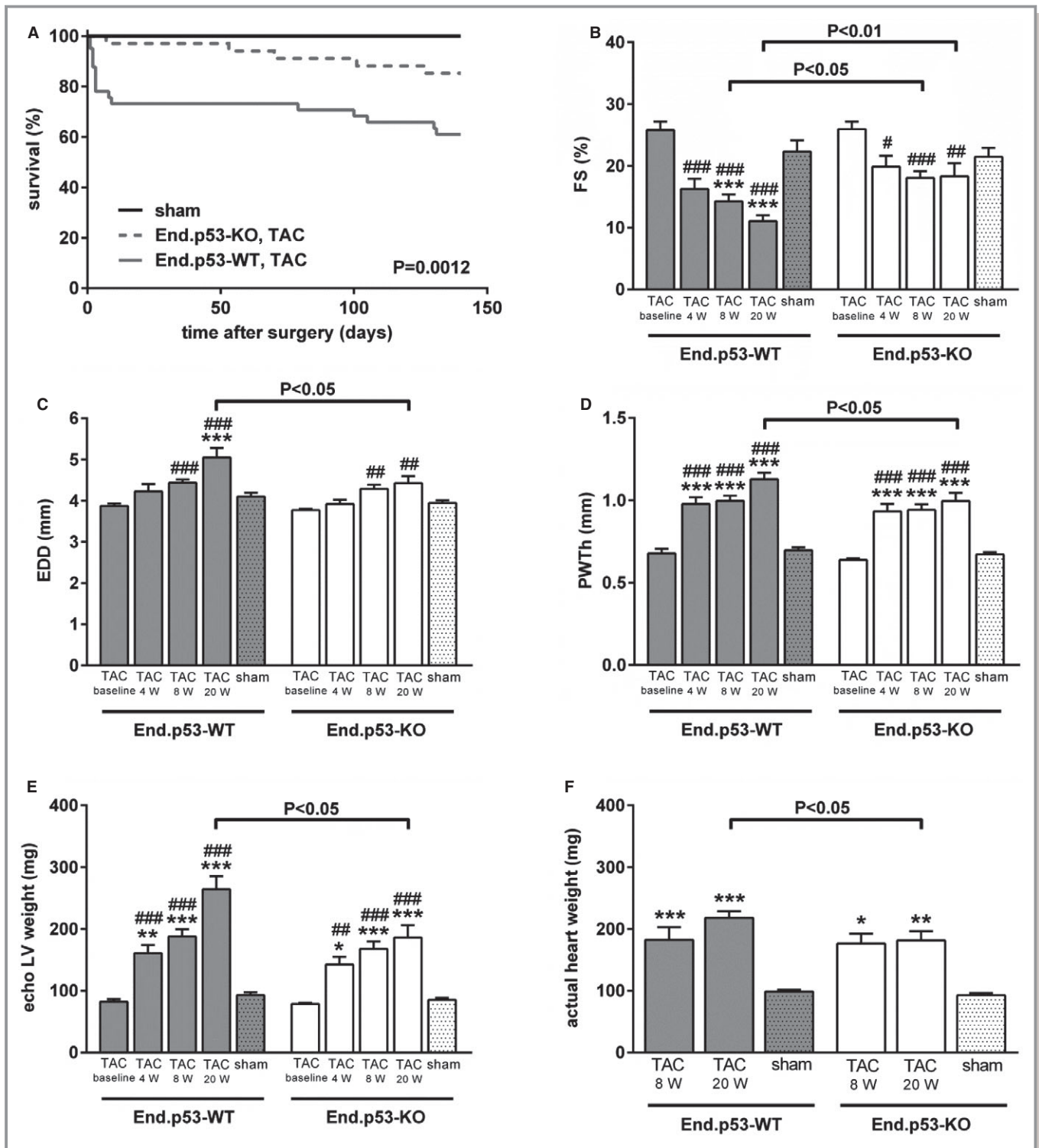
Figure 3. Effect of endothelial p53 deletion on survival and cardiac hypertrophy and function. A, Kaplan–Meier survival analysis of sham-(n=19; n=12 End.p53-WT and n=7 End.p53-KO) or TAC-operated End.p53-WT (n=41) and End.p53-KO (n=34) mice. Mean values for fractional shortening (FS; B), enddiastolic inner LV diameters (EDD; C), posterior wall thickness (PWTh; D), LV weight, determined by echocardiography (E), and actual heart weight, determined at necropsy (F), at baseline and different time points after TAC or sham operation are shown. *P<0.05, **P<0.01 and ***P<0.001 vs sham, #P<0.05, ##P<0.01 and ###P<0.001 vs baseline. Significant differences between End.p53-WT and End.p53-KO mice at specific time points after TAC are indicated within the graphs. TAC indicates transverse aortic constriction.
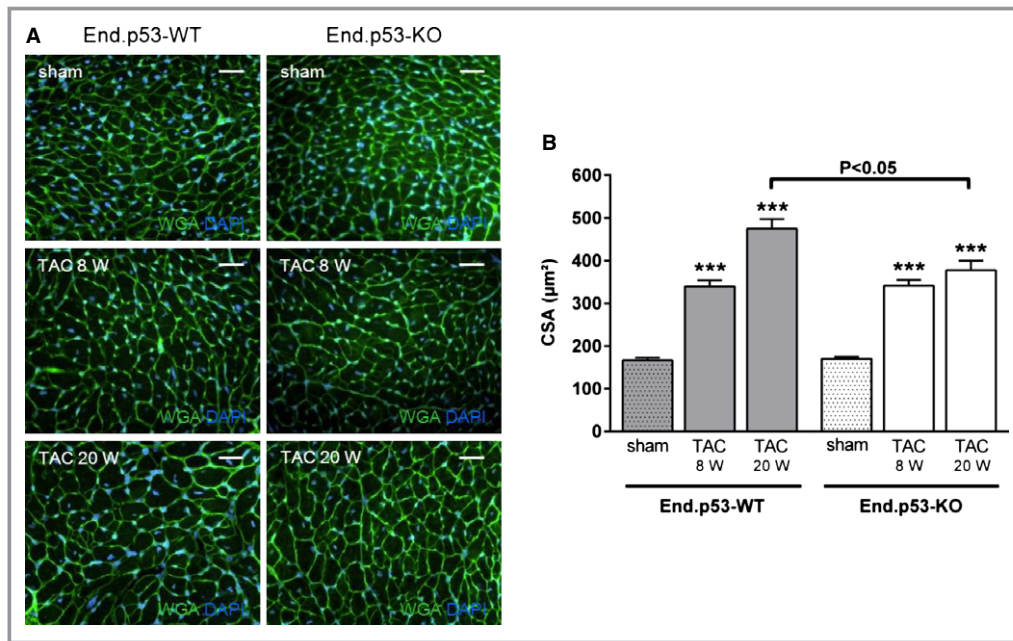
Figure 4. Effect of endothelial p53 deletion on single cardiomyocyte hypertrophy. Representative pictures of WGA-stained myocardial cross sections (A) and the results after quantification of the cardiomyocyte cross-sectional area (CSA; n=7 to 16 mice per group; B) are shown. Size bars represent 100 μm. Grey bars: End.p53-WT mice; white bars: End.p53-KO mice; dotted bars: sham-operated mice. ***$P<0.001$ vs sham. Significant differences between End.p53-WT and End.p53-KO mice are indicated within the graphs. WGA indicates wheat germ agglutinin.

Endothelial p53 Deletion Reduces Apoptosis in Endothelial And Non-Endothelial Cells After TAC

Cardiac hypertrophy is known to be associated with p53 accumulation.[9,10] Our analyses confirmed elevated p53 expression in banded hearts of End.p53-WT mice, whereas cardiac p53 mRNA (Figure 5A) and protein (Figures 5B and 5C) levels were significantly lower in End.p53-KO compared with End.p53-WT mice, particularly at 8 weeks after TAC. Fluorescence microscopy analysis confirmed reduced numbers of p53-immunopositive lectin-positive endothelial, but also lectin-negative cells in banded hearts from End.p53-KO compared with End.p53-WT mice (Figures 5D through 5F). Moreover, lower numbers of activated caspase-3 (Figures 6A through 6C) or TUNEL (Figures 6D through 6F) positive cells were detected in hearts of End.p53-KO compared with End.p53-WT mice after TAC. Quantitative real-time PCR analysis revealed reduced cardiac expression levels of p21, a cyclin-dependent kinase inhibitor and downstream target of p53, and of p53-upregulated modulator of apoptosis (Puma) as well as increased levels of proliferating cell nuclear antigen (Pcna; Figure 7), suggesting that endothelial deletion of p53 reduces cell cycle arrest and apoptotic cell death in hearts after pressure overload.

Deletion of p53 in Endothelial Cells Promotes Cardiac And Extracardiac Angiogenesis

To determine whether deletion of p53 in endothelial cells is able to stabilize the cardiac microvasculature during experimental hypertrophy, the number of CD31-positive endothelial cells (Figures 8A and 8B) and the endothelial lectin-perfused area (Figures 8A and 8C) were quantified revealing a progressive decrease of functional (ie, endothelial lectin-perfused) capillaries in hearts from End.p53-WT mice after TAC, whereas cardiac vascularization was significantly better in End.p53-KO mice 8 weeks and similar to sham-operated littermates 20 weeks after TAC. Expression of the hypoxia marker CAIX was increased in banded hearts of mice of both genotypes, but to a significantly lesser extent in End.p53-KO mice (Figures 8D and 8E). An improved reperfusion (Figures 9A and 9B) and increased capillary density (Figures 9C and 9D) within ischemic muscles from End.p53-KO compared with End.p53-WT mice was also observed after induction of unilateral hindlimb ischemia in males. Modulation of p53 using the nonpeptidic small-molecule nutlin-3a (stabilizing p53 by inhibiting the mdm2-p53 interaction) or pifithrin-α (reducing p53 activity) followed by the analysis of HCMEC sprouting also supported a direct role for p53 during angiogenic processes (Figure 10).
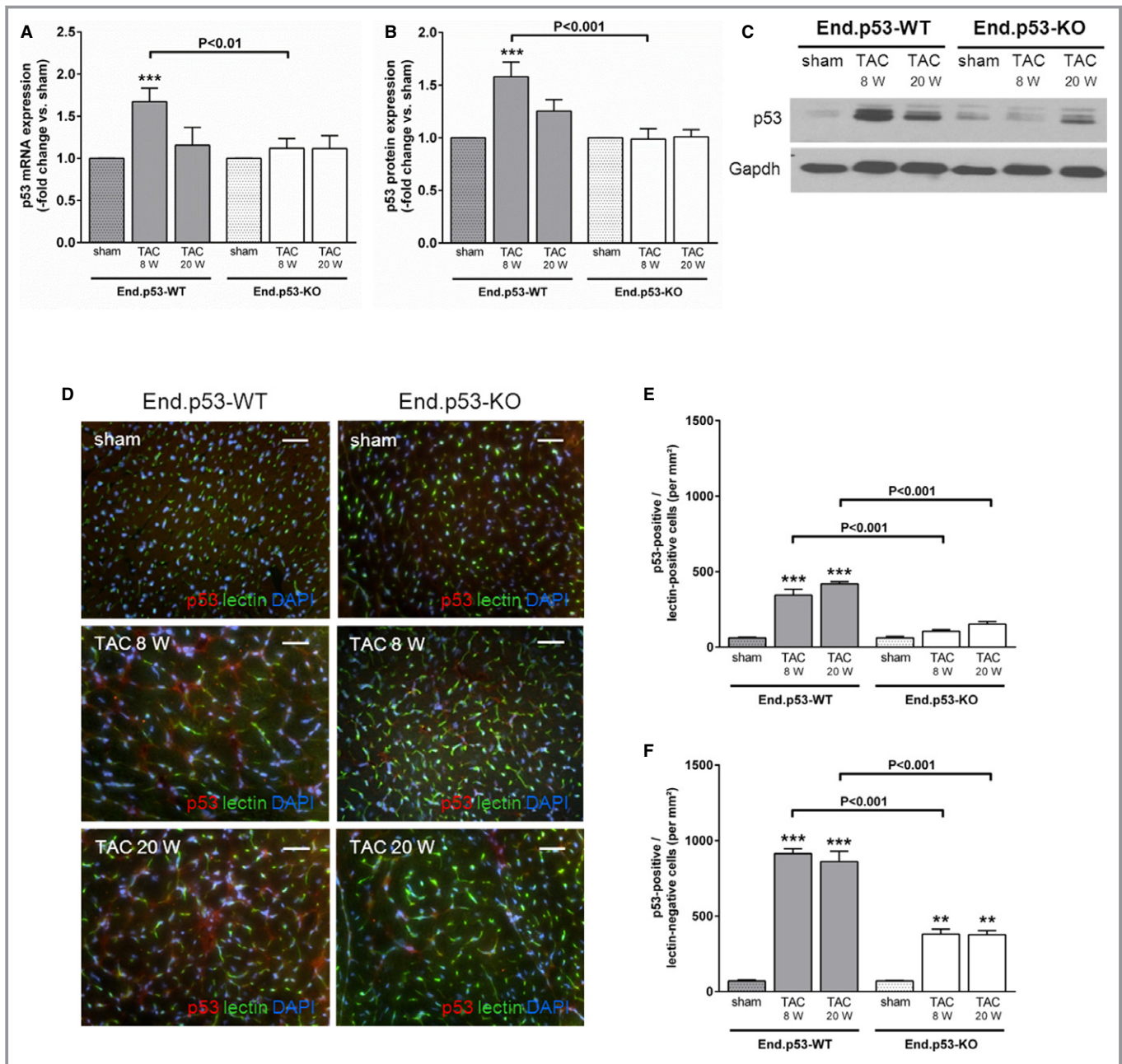
Figure 5. Expression of p53 in sham and TAC-operated mouse hearts. The relative cardiac mRNA and protein expression levels of p53 were analyzed using quantitative qPCR (A) or western blot (B, representative western blot findings are shown in C) in End.p53-WT (grey bars) and End.p53-KO mice (white bars) (n=8 to 19 mice per group). Results were normalized to Gapdh and expressed as -fold change vs sham-operated littermates of the same genotype (set at 1; dotted bars). D through F, Cardiac cross sections were examined for the expression of p53. Intravitally isolectin B4 perfused capillaries are green, DAPI-positive cell nuclei blue. Representative pictures of findings in End.p53-WT and End.p53-KO mice after sham or TAC surgery are shown in (D). Size bars represent 100 μm. The summary of findings in n=4 to 6 mice per group is shown in (E and F). **P<0.01 and ***P<0.001 vs sham. Significant differences between End.p53-WT and End.p53-KO mice are indicated within the graphs. PCR indicates polymerase chain reaction; DAPI,4′,6-diamidino-2-phenylindole; TAC, transverse aortic constriction.

Deletion of p53 in Endothelial Cells is Associated With Elevated Hif1α And Vegf Levels

Cardiac p53 accumulation was shown to be involved in hypoxia-independent Hif1α degradation and angiogenesis inhibition following pressure overload.[15] To examine potential mechanisms underlying the proangiogenic effects of endothelial p53 deletion (in addition to reducing cell cycle arrest and apoptotic cell death), we examined Hif1α and Vegf protein levels in pressure-overloaded hearts of End.p53-WT
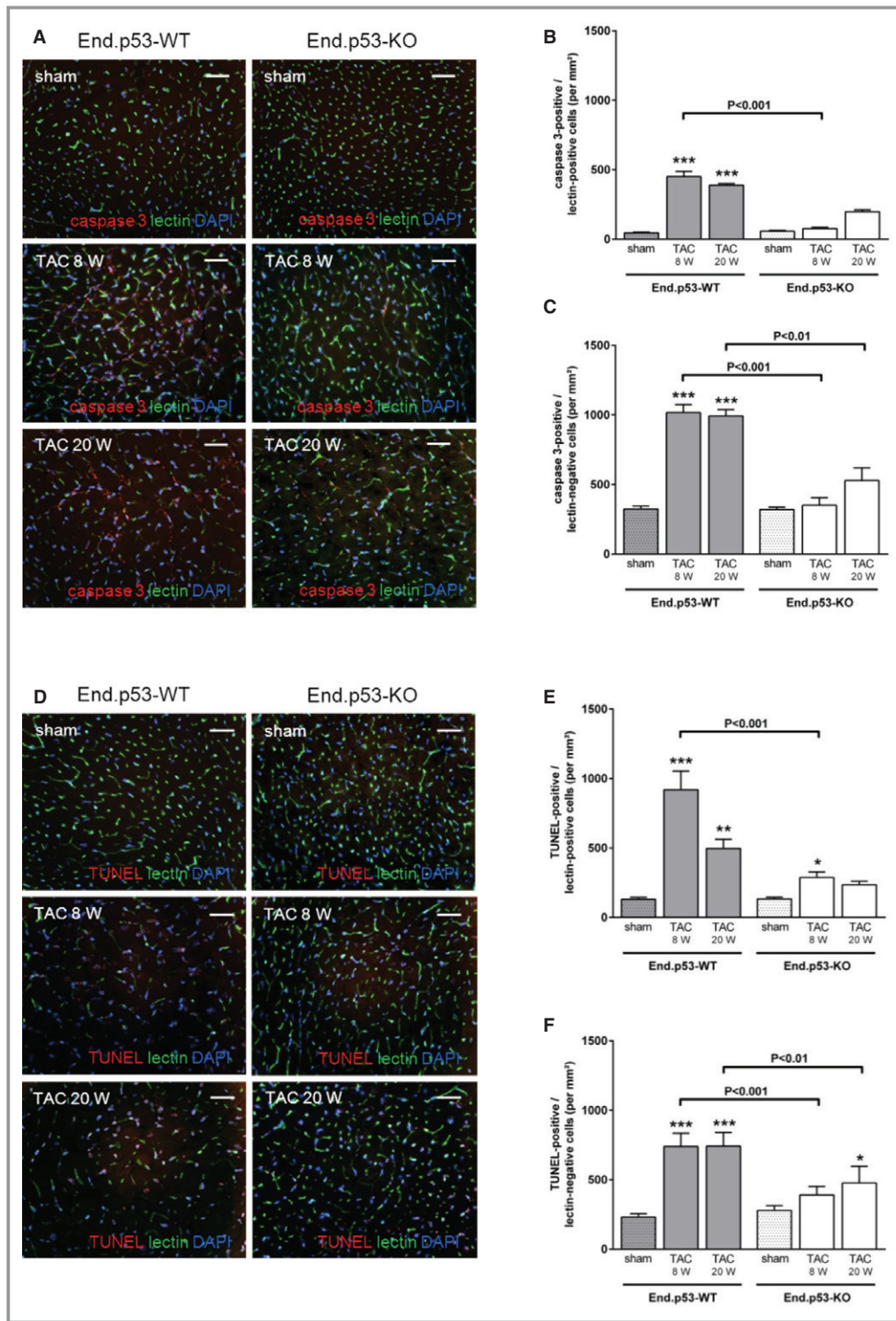
Figure 6. Analysis of apoptosis in sham and TAC-operated mouse hearts. Cardiac cross sections were examined for activated caspase-3 (A through C) or TUNEL (D through F). Intravitally isolectin B4 perfused capillaries are green, DAPI-positive cell nuclei blue. Representative pictures of findings in End.p53-WT and End.p53-KO mice (n=3 to 8 per group) are shown in (A and D). Size bars represent 100 µm. *$P<0.05$, **$P<0.01$ and ***$P<0.001$ vs sham. Significant differences between End.p53-WT and End.p53-KO mice are indicated within the graphs. TAC indicates transverse aortic constriction; DAPI, 4′,6-diamidino-2-phenylindole.
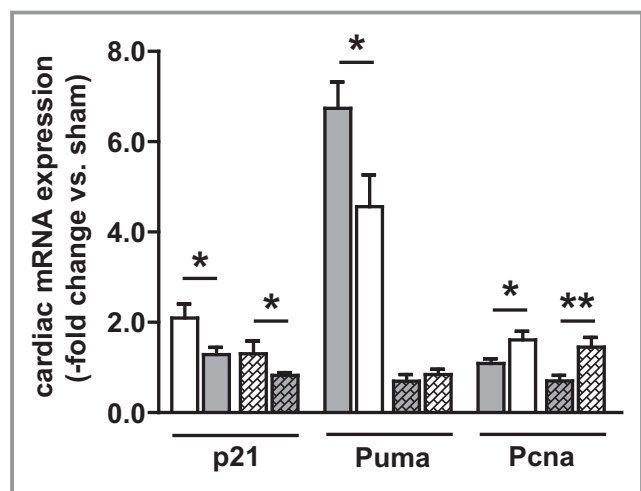
Figure 7. Expression of p53 target genes involved in cell cycle control, apoptosis and proliferation in sham and TAC-operated mouse hearts. The relative cardiac mRNA expression levels of p21, p53 upregulated modulator of apoptosis (Puma) and proliferating cell nuclear antigen (Pcna) were analyzed using quantitative qPCR in End.p53-WT (grey bars) and End.p53-KO mice (white bars) (n=8 to 19 mice per group). Results were normalized to Gapdh and expressed as -fold change vs sham-operated littermates of the same genotype (set at 1; not shown). *$P<0.05$ and **$P<0.01$ vs End.p53-WT. PCR indicates polymerase chain reaction; TAC, transverse aortic constriction.

and End.p53-KO mice. At 8 and 20 weeks after TAC, Hif1α (Figures 11A and 11B) and Vegf (Figures 11A and 11C) levels were significantly elevated in End.p53-KO mice, whereas no changes were observed in End.p53-WT animals. Analyses at earlier time points (ie, 7 days after TAC) revealed elevated Hif1α protein levels in both genotypes and confirmed that the TAC-induced increase in Hif1α and Vegf expression was significantly more pronounced in mice lacking p53 in endothelial cells (Figures 11D through 11F). Analysis of HCMECs, stably transduced with lentiviral vectors containing either scr or p53 shRNA followed by the exposure to CoCl$_2$ confirmed that endothelial deletion of p53 significantly increased Hif1α protein levels in response to (chemical) hypoxia (Figures 11G and 11H). Overall, these data suggested that reduced Hif1α degradation and increased Vegf expression may have contributed to the proangiogenic effects of endothelial p53 deletion.

Endothelial p53 Deletion Attenuates Pressure Overload-Induced Cardiac Fibrosis

To examine the effects of improved cardiac vascularization in mice with endothelial p53 deletion on cardiac remodeling processes after TAC, cardiac cross sections were examined after staining with Masson's trichrome. Whereas fibrosis was negligible in sham-operated mice, multiple scattered foci of

interstitial fibrosis were observed in End.p53-WT and to a significantly lesser extent in End.p53-KO mouse hearts, both at 8 and 20 weeks after TAC (Figures 12A and 12B). Picrosirius red staining confirmed lower amounts of interstitial collagen in hearts of TAC-operated End.p53-KO compared with End.p53-WT mice (not shown). Also, immunohistochemistry demonstrated reduced expression of collagen 1A1 (col1A1) and fibroblast-specific protein1 (Fsp1) in banded hearts of End.p53-KO mice compared with their End.p53-WT counterparts and lower numbers of cells double-immunopositive for either of the mesenchymal markers and the endothelial marker CD31 (Figure 13).

Quantitative *real-time* PCR analysis revealed lower cardiac mRNA levels of collagen type I alpha 1 (Col1a1) and vimentin in End.p53-KO compared with End.p53-WT mice 8 weeks after TAC (Figure 12C). Altered expression levels of p53 target genes involved in ECM turnover, such as bone morphogenetic protein (Bmp)-7 (Figure 12D), connective tissue growth factor (Ctgf) or plasminogen activator inhibitor (Pai)-1 (Figure 12E), were detected in hearts of mice lacking endothelial p53 suggesting that both reduced production and enhanced degradation of ECM proteins may be involved in the attenuated fibrosis observed in End.p53-KO mouse hearts. Also, lower mRNA expression levels of the transcription factors Snail, Slug, and Twist, controlling mesenchymal differentiation, were detected in banded hearts of mice with endothelial p53 deletion compared with their WT counterparts (Figures 14A through 14C). Similar findings were observed after TGFβ$_1$ stimulation of HCMECs, stably transfected with scr or p53 shRNA (Figures 14D through 14E), or in the presence or absence of nutlin-3a or pifithrin-α (Figure 15). Of note, immunofluorescence analysis revealed a similar increase in the number of CD45-positive inflammatory cells in banded hearts of End.p53-WT and End.p53-KO mice (457±36 and 439±10 cells per mm² at 7 days after TAC; P=n.s.) compared with sham-operated mice (41±16 and 55±19 cells per mm²), minimizing the possibility that differences in cardiac inflammation may have contributed to the observed reduction in cardiac fibrosis in End.p53-KO mice.

Discussion

In this study, we examined the importance and causal role of endothelial p53 expression for cardiac remodeling processes and the development of heart failure induced by chronic pressure overload in mice. Our main findings are that inducible deletion of p53 in endothelial cells of adult mice prevents the rarefaction of capillary endothelial cells observed with developing heart failure and is associated with reduced apoptotic death of cardiac endothelial, but also non-endothelial cells. In addition to improving cardiac perfusion and
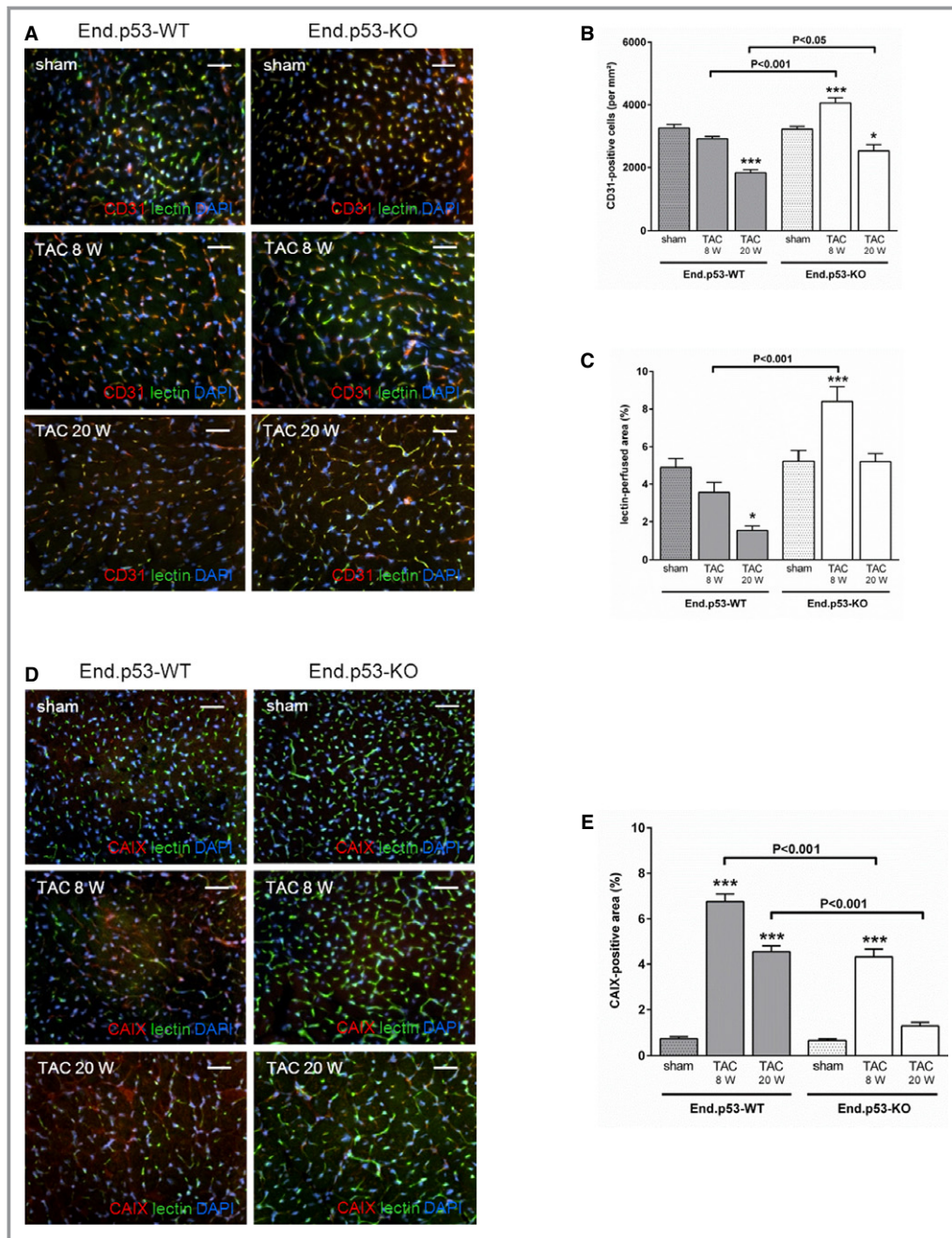
Figure 8. Cardiac vascularization in End.p53-WT and End.p53-KO mice. A, Representative pictures of CD31-immunopositive, isolectin B4-perfused capillaries in hearts of sham- or TAC-operated End.p53-WT and End.p53-KO mice. B, Quantification of CD31-positive cells per mm^2. C, Quantification of the lectin-positive area. D, Immunostaining for CAIX to visualize cardiac hypoxia. Size bars represent 100 μm. E, The summary of the quantitative analysis in n=4 to 9 mice per group. *$P<0.05$ and ***$P<0.001$ vs sham. Significant differences between End.p53-WT and End.p53-KO mice are indicated within the graphs. TAC indicates transverse aortic constriction.

diminishing the extent of pressure overload–induced cardiac hypoxia thus preventing replacement fibrosis, endothelial p53 deletion was found to beneficially alter the cardiac expression of factors involved in ECM production and turnover (in particular, Bmp7, Ctgf, and Pai-1) and the control of

mesenchymal differentiation (eg, Snail, Slug, and Twist). As a result, endothelial p53 deletion attenuated the progressive LV dilation and systolic pump dysfunction present in End.WT-p53 mice and improved survival. Thus, our data support the importance of endothelial cells during pressure overload–
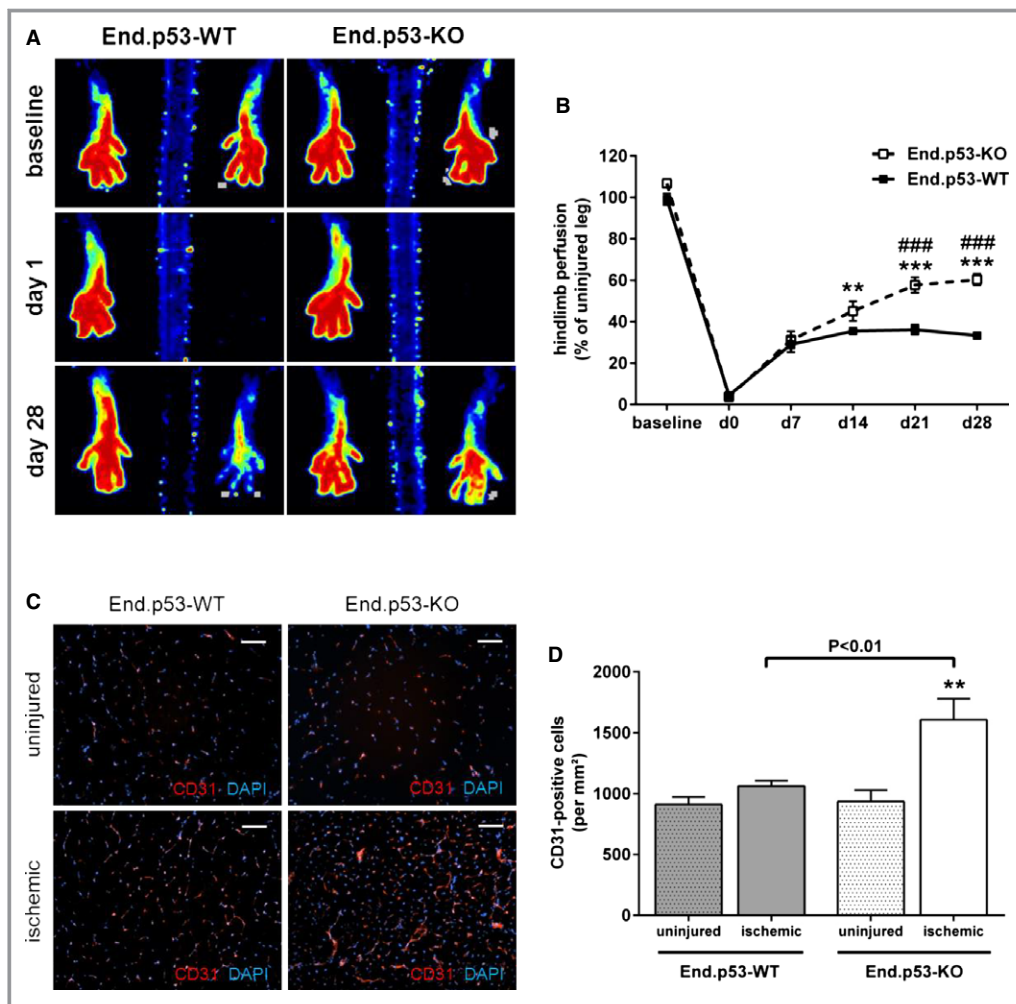
Figure 9. Effect of endothelial p53 deletion on new vessel formation following hindlimb ischemia. A, Representative laser Doppler perfusion images before as well as on day 1 and 28 after unilateral hindlimb ischemia in End.p53-WT and End.p53-KO mice. B, Summarized findings in End.p53-WT (n=16) and End.p53-KO mice (n=14). **$P<0.01$ and ***$P<0.001$ vs baseline; ###$P<0.001$ vs End.p53-WT mice. C, Representative pictures of CD31-immunopositive endothelial cells in cryosections through the gastrocnemic muscle. Cell nuclei were counterstained with DAPI. Size bars represent 100 μm. D, Quantitative analysis of the capillary density 28 days after ischemia (n=8 to 10 mice per group). **$P<0.01$ vs the contralateral, uninjured leg. Significant differences between End.p53-WT and End.p53-KO mice are indicated within the graph; DAPI indicates 4′, 6-diamidino-2-phenylindole.

induced cardiac remodeling and suggest a direct link between endothelial p53 expression, cardiac angiogenesis, and fibrosis.

The tumor suppressor protein p53 is activated in response to a variety of cellular stress signals. DNA damage, but also oxidative stress, hypoxia, or cytokine stimulation may induce apoptotic cell death via p53 and transcriptional activation of genes involved in cell cycle control and growth arrest.[24] A role for p53 in the pathogenesis of heart disease is supported by findings of increased apoptotic cell numbers and p53 protein levels in the myocardium of patients with advanced heart disease,[10] correlating with the transition to heart failure.[9] Activation of p53 and associated genes was also reported in

experimental rat,[11] sheep,[25] or dog[26] models of heart failure. Of note, quantitative analysis of TUNEL-positive cells in banded mouse hearts revealed 0.7% apoptotic cardiomyocytes and 1% apoptotic non-cardiomyocytes, half of which were identified as CD31-positive endothelial cells.[17] Activation of p53 may be causally involved in the development of heart failure. For example, mice with global p53 deficiency are characterized by increased cardiac angiogenesis and protection from acute TAC- or myocardial infarction-induced heart failure.[15] Similar findings were observed in mice systemically treated with the synthetic p53 inhibitor pifithrin-α.[13] Overexpression of CHIP, an endogenous p53 inhibitor, prevented myocardial apoptosis, and ameliorated ventricular remodeling
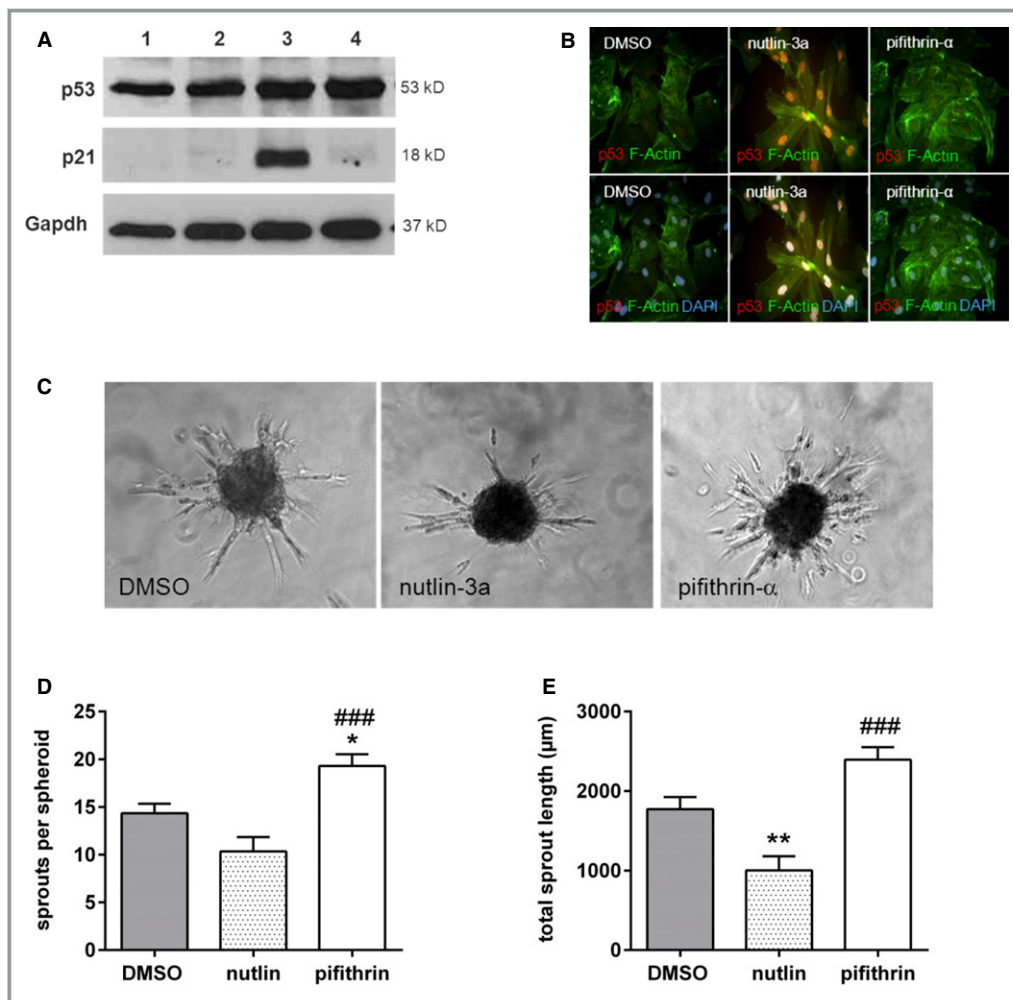
Figure 10. Effect of p53 modulation on the angiogenic properties of endothelial cells in vitro. A, Representative western blot membranes showing the expression of p53 or its downstream effector p21 after incubation of human cardiac microvascular endothelial cells (HCMECs) with either PBS (1), vehicle (DMSO; 2), nutlin-3a (10 µmol/L; 3) or pifithrin-α (20 µmol/L; 4). Gapdh was used as internal control for equal protein loading. B, Representative pictures of HCMECs treated with either DMSO, nutlin-3a or pifithrin-α, followed by immunodetection of p53. C, Representative pictures of HCMEC spheroids after treatment with either DMSO, nutlin-3a or pifithrin-α. Magnification, ×200. D and E, Summary of the quantitative and statistical analysis. The number of sprouts (D) or the total sprout length (E) per spheroid were calculated using ImagePro Plus image analysis software. *$P<0.05$ and **$P<0.01$ vs DMSO; ###$P<0.001$ vs nutlin-3a, as determined using ANOVA. ANOVA indicates analysis of variance; DMSO, dimethyl sulfoxide.

after myocardial infarction.[27] Global p53 deficiency[14] as well as cardiomyocyte-specific expression of dominant-negative p53[28] also protected against the cardiotoxic effects of doxorubicin, although a recent study in mice with cardiomyocyte-specific p53 deletion did not observe any cardioprotection.[29] In addition to the possibility that doxorubicin-induced apoptosis occurs in a p53-independent manner, the latter findings may also suggest that expression of p53 in other cell types (eg, endothelial cells, but also inflammatory or smooth muscle cells) may be more important. Supporting a role for endothelial p53, circulating levels of growth differentiation factor-15, a cytokine

induced in the heart during ischemia or pressure overload and shown to reflect p53 activation in endothelial cells,[30] were found to provide independent prognostic information in patients with advanced heart failure.[31] However, the cardioprotective effects of endothelial cell-specific p53 deletion have not been directly addressed so far.

Endothelial cell apoptosis is a well-known anti-angiogenic mechanism. It occurs during vascular pruning, ie, the removal of aberrant neovessels, and represents a vital step during secondary vascular network formation. Angiogenesis inhibitors have been shown to promote apoptosis,[32] whereas
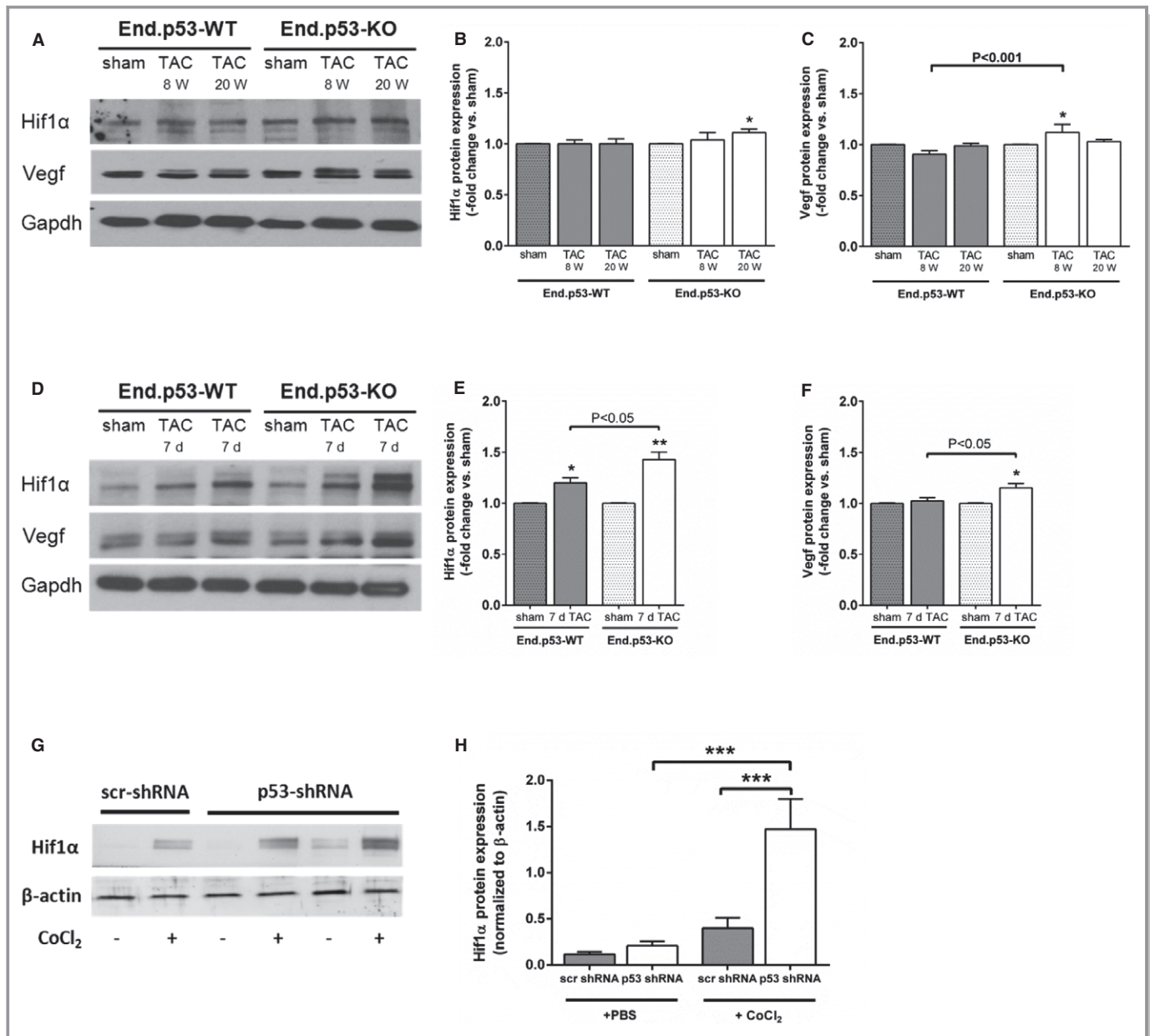
Figure 11. Effect of endothelial p53 deletion on Hif1α and Vegf levels. A through F, Western blot analysis of cardiac Hif1α and Vegf protein levels in End.p53-WT and End.p53-KO mice at different time points after transverse aortic constriction (TAC) or sham operation (S). Representative membranes are shown in A (8 and 20 weeks after TAC) and D (7 days after TAC). *P<0.05 and **P<0.01 vs sham. Significant differences between End.p53-WT and End.p53-KO mice are indicated within the graphs. G and H, Analysis of Hif1α protein levels in HCMECs after stable transfection with lentiviral p53 shRNA or negative control vector (scr shRNA) and exposure to chemical hypoxia (1 mmol/L CoCl₂ for 4 h). Representative findings are shown in G, the results of the quantitative analysis of n=3 independent experiments in H. ***P<0.001.

angiogenic growth factors (including Vegf) protect endothelial cells from programmed cell death.[33] Previous studies have shown that overexpression of p53 inhibits endothelial differentiation and angiogenesis.[34] Possible mechanisms include the transcriptional activation of angiogenesis inhibitors, such as collagen prolyl hydroxylase[35] or increased production of Mmp2 or Mmp9 resulting in the release of anti-angiogenic factors.[36] In the present study, elevated cardiac expression of

Mmp9 and reduced levels of the MMP inhibitor Pai-1 were observed in hearts of End.p53-KO mice. In addition, p53 accumulation was shown to interfere with hypoxia-sensing systems and to promote the proteosomal degradation of Hif1α resulting in impaired Vegf expression, cardiac angiogenesis and LV dysfunction, despite the presence of hypoxia.[15] Similarly, angiotensin II was shown to impair cardiac angiogenesis via p53-dependent downregulation of
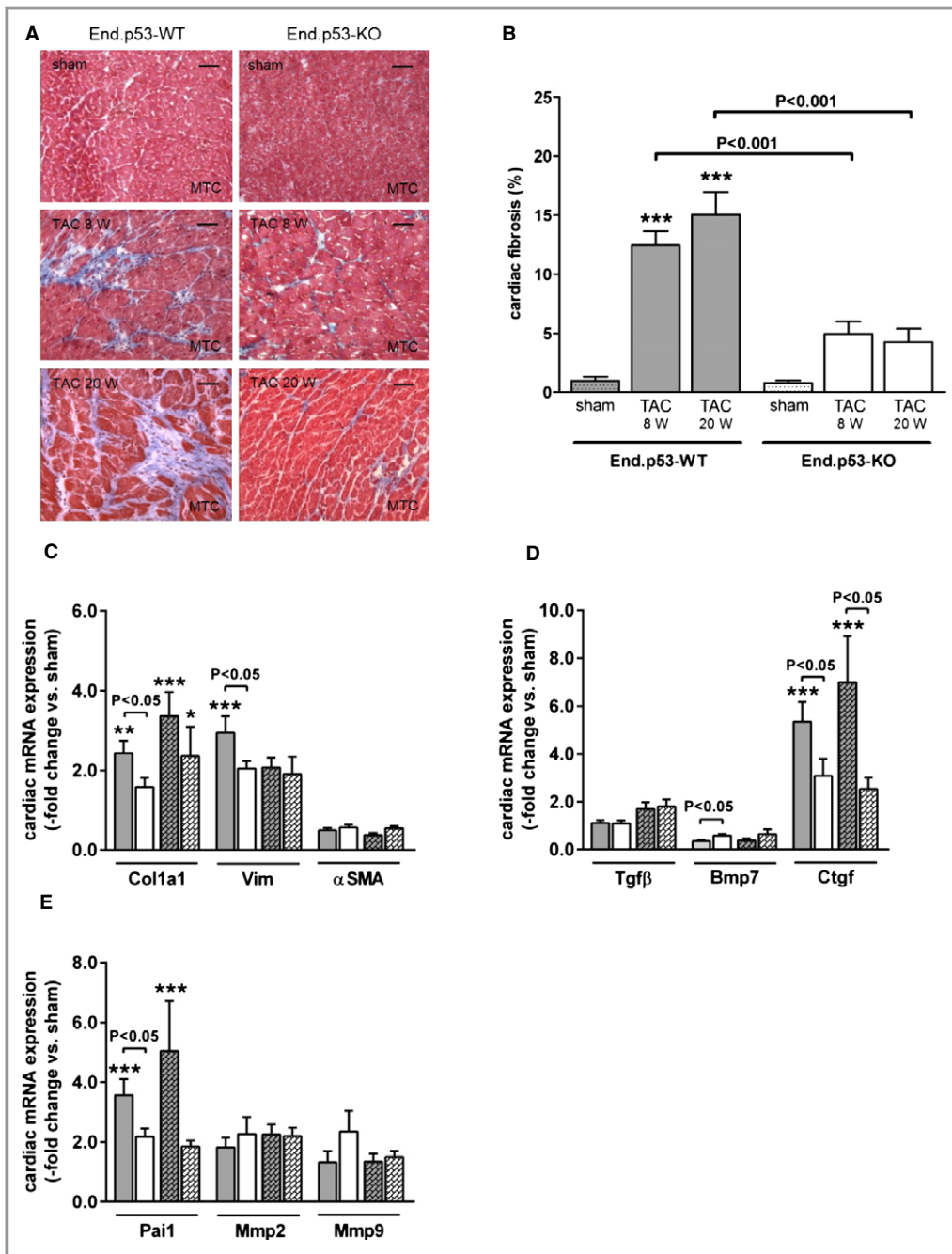
Figure 12. Effect of endothelial p53 deletion on cardiac fibrosis. A, Representative images after MTC staining of hearts from End.p53-WT and End.p53-KO mice. Size bars represent 200 μm. B, Summary of the quantitative analysis in n=7 to 15 mice per group. Quantitative qPCR analysis of the mRNA levels of ECM proteins and mesenchymal markers (C), or factors involved in ECM production (D) and degradation (E). Grey bars: End.p53-WT mice; white bars: End.p53-KO mice; open bars: 8 W after TAC; cross-hatched bars: 20 W after TAC. Results were normalized to Gapdh and are expressed as -fold increase vs sham-operated mice (set at 1; not shown). *$P<0.05$, **$P<0.01$ and ***$P<0.001$ vs sham. Significant differences between End.p53-WT and End.p53-KO mice are indicated within the graphs. PCR indicates polymerase chain reaction; TAC, transverse aortic constriction.

Hif1α.[37] In line with these previous findings, our analyses revealed that p53 deletion in endothelial cells was associated with elevated Hif1α and Vegf levels in response to pressure overload in vivo or hypoxia in vitro, both of which may have contributed to the observed stabilization of the cardiac vasculature.
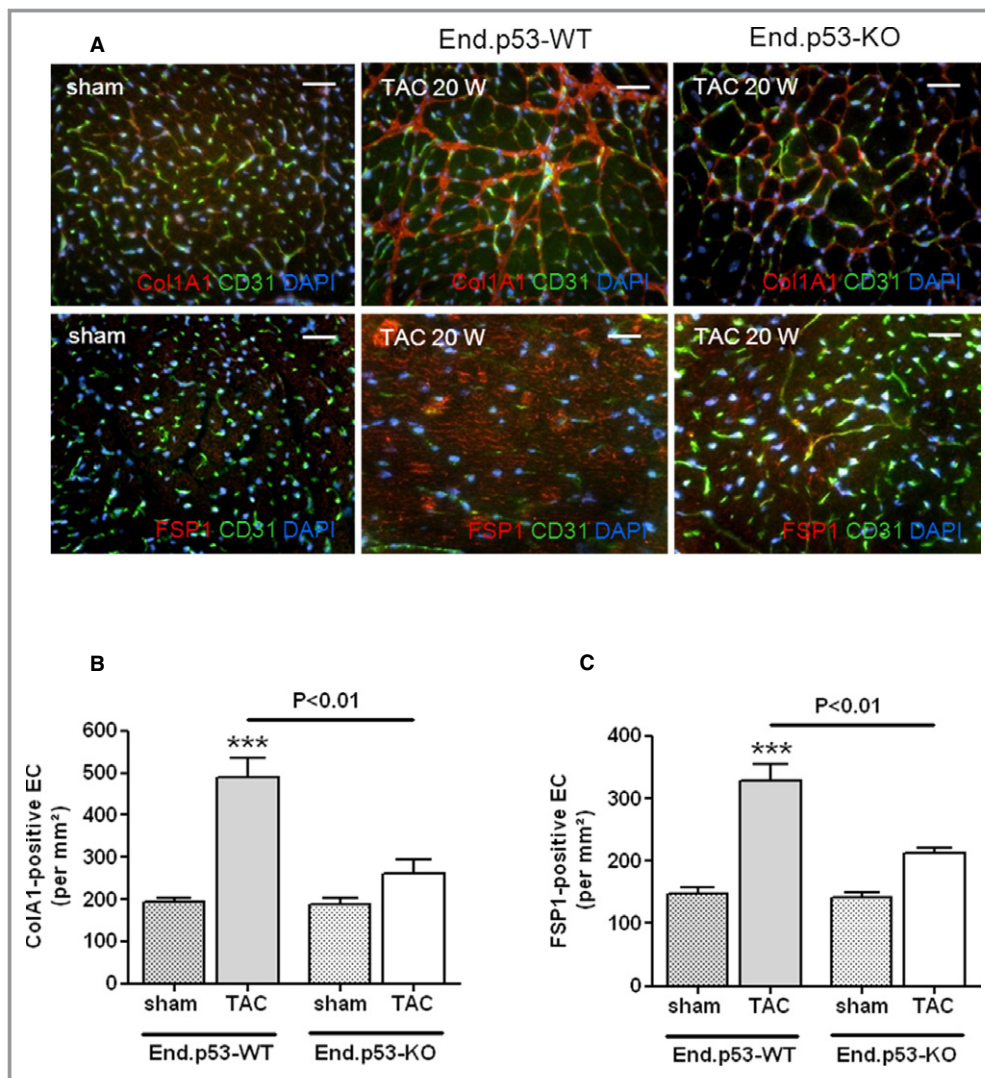
Figure 13. Co-localization of endothelial and mesenchymal markers in hearts of sham and TAC-operated mice. A through C, Representative images (A) and summarized findings after quantification of Col1A1$^+$/CD31$^+$ (B) and Fsp-1$^+$/CD31$^+$ cells (C) in hearts of sham- or TAC-operated End.p53-WT and End.p53-KO mice (n=3 to 6). Size bars represent 100 μm. ***P<0.001 vs sham. Significant differences between End.p53-WT and End.p53-KO mice are indicated within the graph. TAC indicates transverse aortic constriction.

Several studies have shown that the progression of cardiac hypertrophy towards heart failure is associated with rarefaction of the cardiac microvasculature, which is then unable to support the increased oxygen and nutrient demands of the hypertrophied myocardium.[1–3] Building on these previous findings, we could now show that deletion of p53 in endothelial cells prevents the reduction in cardiac capillary density after TAC resulting in enhanced perfusion of the hypertrophied heart. The anti-angiogenic effects of p53 could be confirmed in vitro as well as after induction of unilateral hindlimb ischemia in vivo. Importantly, our findings also suggest that prevention of endothelial cell cycle arrest and stabilization of cardiac capillaries may delay the progressive LV dilation and the decline of systolic pump

function. In contrast to previous studies showing that augmentation of angiogenesis promotes myocardial hypertrophy even in the absence of an initiating stimulus,[8] endothelial p53 deletion was found to be associated with a reduced extent of cardiac hypertrophy at later time points (ie, 20 weeks after TAC), as determined by wall thickness, heart weight, or cardiomyocyte area. Future studies will have to examine in more detail how the cross-talk between endothelial cells and cardiomyocytes during hypertrophy may be affected by p53.

Hearts of End.p53-KO mice exhibited markedly reduced fibrosis and expressed lower amounts of collagen type I and other mesenchymal markers, which may have contributed to the preservation of cardiac pump function. Possible
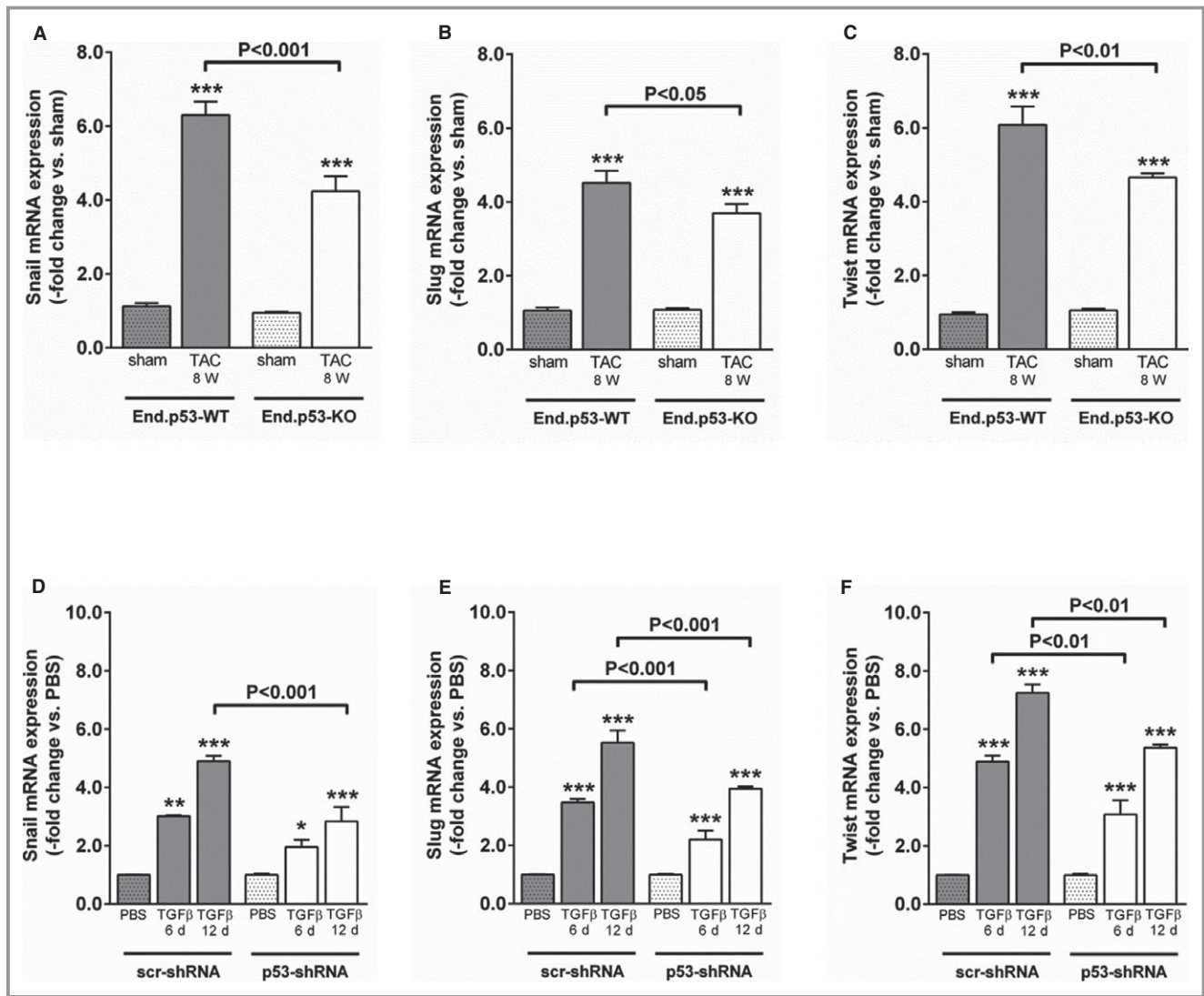
Figure 14. Effect of endothelial p53 deletion on transcription factors involved in mesenchymal differentiation. A through C, qPCR analysis of whole mouse hearts (n=9 per group) from End.p53-KO (white bars) and End.p53-WT mice (grey bars) 8 weeks after TAC for Snail (A), Slug (B) and Twist (C) mRNA. ***$P<0.001$ vs sham. D through F, HCMECs were stable transfected with lentiviral p53-shRNA or negative control (scr) shRNA vector, treated with PBS or TGFβ1 (10 ng/mL) for 6 or 12 days and the expression of transcription factors regulating mesenchymal differentiation examined by qPCR analysis. *$P<0.05$, **$P<0.01$ and ***$P<0.001$ vs PBS-treated cells (n=3 to 6 separate experiments). Significant differences between p53 shRNA and scr shRNA transfected cells are indicated within the graphs. HCMEC indicates human cardiac microvascular endothelial cells; PCR, polymerase chain reaction; TAC, transverse aortic constriction; TGFβ, transforming growth factor-beta.

mechanisms underlying the reduced cardiac fibrosis in mice lacking p53 in endothelial cells may include indirect effects, such as improved cardiac perfusion limiting hypoxia (as shown by the surrogate marker CAIX) and the death of adjacent cardiomyocytes. In this regard, reduced numbers of activated caspase-3 and TUNEL-positive endothelial lectin–positive as well as endothelial lectin–negative cells (presumably cardiomyocytes, fibroblasts, or smooth muscle cells) were observed in hearts of End.p53-KO mice. On the other hand, differences in inflammatory cell recruitment are not likely involved in the observed differences in cardiac fibrosis. Also, we observed no

differences in cardiac eNOS expression between both genotypes (not shown), which may have contributed to the reduced cardiac fibrosis in End.p53-KO mice.[38] Several genes involved in ECM synthesis and degradation are known to be directly regulated by p53 and may have acted in a paracrine manner on adjacent cardiomyocytes and/or fibroblasts.[16] For example, End.p53-KO mouse hearts expressed significantly lower amounts of Ctgf, a major regulator of tissue fibrosis, and elevated Ctgf expression and increased liver fibrosis was reported in mice with hepatocyte-specific p53 activation.[39] Moreover, the p53-regulated factors Pai-1 and Mmp9 are not
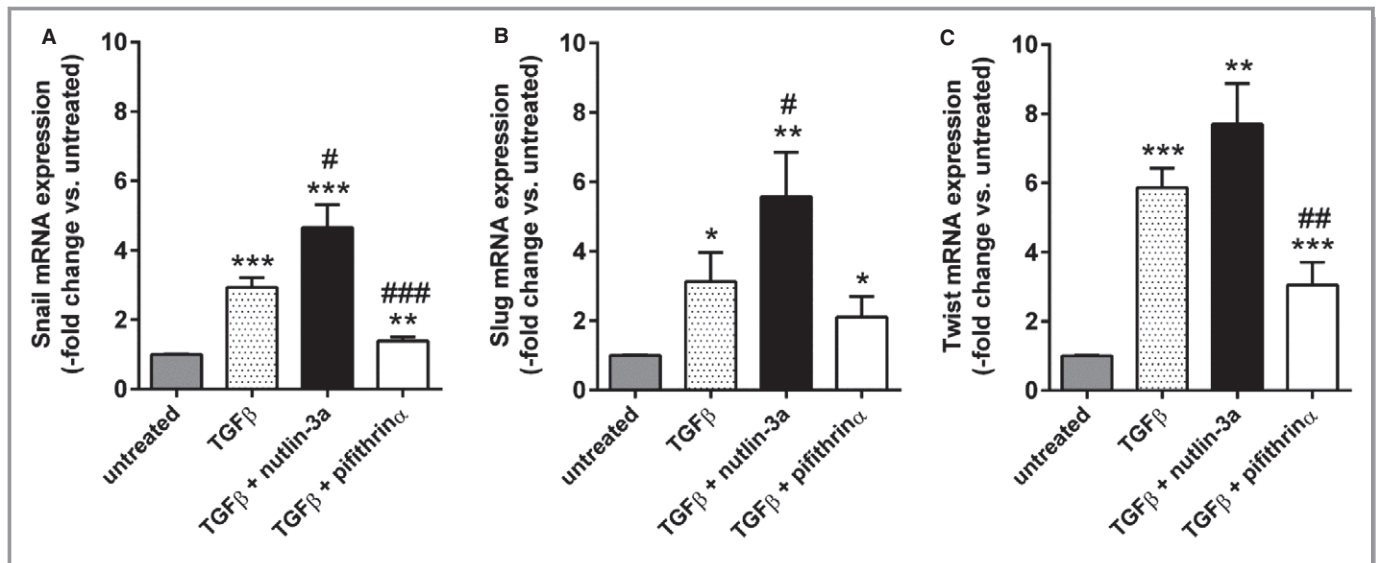
Figure 15. Effect of p53 activation or inhibition on the TGFβ-induced expression of the transcription factors Snail, Slug, and Twist. A through C, Quantitative *real-time* PCR analysis of the transcription factors and EndMT surrogate markers Snail (A), Slug (B) and Twist (C) mRNA expression in human cardiac microvascular endothelial cells (HCMECs) after treatment with TGFβ1, alone or in combination with nutlin-3a (to stabilize p53) or pifithrin-α (to inhibit p53 activity) for 6 days. Similar findings were observed after treatment for 12 days (not shown). *$P<0.05$, **$P<0.01$ and ***$P<0.001$ vs untreated cells; #$P<0.05$, ##$P<0.01$ and ##$P<0.001$ vs TGFβ1-treated cells. PCR indicates polymerase chain reaction; TGFβ, transforming growth factor-beta.

only involved in the proteolytic release of angiogenesis inhibitors, but also modulate ECM degradation. Of note, constitutive deletion of p53 in endothelial cells was reported to be associated with a worse outcome and more severe cardiac fibrosis in mice after total body irradiation,[25] and differences in the type of injury may underlie this discrepancy. Reduced numbers of Col1A1^{+}/CD31^{+} and Fsp1^{+}/CD31^{+}-double positive cells or mRNA expression of the transcription factors Snail, Slug, and Twist in hearts of End.p53-KO mice after TAC suggest that differences in mesenchymal differentiation may have contributed to the observed protection against cardiac fibrosis in mice lacking endothelial p53, but analyses in endothelial reporter mice, in combination with p53 deletion, are needed to definitively address this point. Previous studies have shown that TGFβ-induced fibroblast activation and EndMT are significant contributors to myocardial fibrosis,[40] although this paradigm has been recently challenged.[41] Although cardiac levels of TGFβ did not differ between both genotypes, elevated levels of Bmp7, shown to preserve the endothelial phenotype and to counteract TGFβ-induced organ fibrosis,[42] were detected in hearts of End.p53-KO mice and might have contributed to our observations.

Our results also suggest that modulating endothelial p53 expression may represent an interesting therapeutic target. In this regard, atorvastatin was found to restore ischemic limb loss in diabetes by activation of the Akt/mdm2 pathway and augmentation of p53 degradation,[43] and modulation of endothelial p53 may also underlie the beneficial effects of statins on markers of endothelial function and LV remodeling

in heart failure patients.[44] Our findings may be especially relevant in elderly subjects, a population at increased risk for heart failure, as aging is associated with elevated levels of p53. For example, prolonged passaging (mimicking senescence) of human vein endothelial cells was associated with p53 accumulation,[45] whereas mice with a truncated p53 mutation resulting in p53 activation exhibited an early-onset phenotype consistent with accelerated aging.[46]

Conclusions

Our findings suggest that accumulation of p53 in endothelial cells contributes to the increased endothelial cell death and rarefaction of cardiac microvasculature during cardiac hypertrophy and promotes the development of cardiac fibrosis and LV dysfunction through, at least in part, impaired cardiac perfusion and altered ECM remodeling. Attenuation of endothelial cell loss and preservation of cardiac vascularization during pathologic hypertrophy may thus represent a promising approach to improve pressure overload-induced cardiac remodeling and to prevent the transition to heart failure.

Acknowledgments

Disclosures

None.

References

1. Hein S, Arnon E, Kostin S, Schonburg M, Elsässer A, Polyakova V, Bauer EP, Klovekorn WP, Schaper J. Progression from compensated hypertrophy to failure in the pressure-overloaded human heart: structural deterioration and compensatory mechanisms. *Circulation*. 2003;107:984–991.

2. Shiojima I, Sato K, Izumiya Y, Schiekofer S, Ito M, Liao R, Colucci WS, Walsh K. Disruption of coordinated cardiac hypertrophy and angiogenesis contributes to the transition to heart failure. *J Clin Invest*. 2005;115:2108–2118.

3. Oka T, Akazawa H, Naito AT, Komuro I. Angiogenesis and cardiac hypertrophy. Maintenance of cardiac function and causative roles in heart failure. *Circ Res*. 2014;114:1565–1571.

4. Giordano FJ, Gerber HP, Williams SP, VanBruggen N, Bunting S, Ruiz-Lozano P, Gu Y, Nath AK, Huang Y, Hickey R, Dalton N, Peterson KL, Ross J, Chien KR, Ferrara N. A cardiac myocyte vascular endothelial growth factor paracrine pathway is required to maintain cardiac function. *Proc Natl Acad Sci USA* 2001;98:5780–5785.

5. Izumiya Y, Shiojima I, Sato K, Sawyer DB, Colucci WS, Walsh K. Vascular endothelial growth factor blockade promotes the transition from compensatory cardiac hypertrophy to failure in response to pressure overload. *Hypertension*. 2006;47:887–893.

6. Friehs I, Margossian RE, Moran AM, Cao-Danh H, Moses MA, del Nido PJ. Vascular endothelial growth factor delays onset of failure in pressure-overload hypertrophy through matrix metalloproteinase activation and angiogenesis. *Basic Res Cardiol*. 2006;101:204–213.

7. Heineke J, Auger-Messier M, Xu J, Oka T, Sargent MA, York A, Klevitsky R, Vaikunth S, Duncan SA, Aronow BJ, Robbins J, Crombleholme TM, Molkentin JD. Cardiomyocyte GATA4 functions as a stress-responsive regulator of angiogenesis in the murine heart. *J Clin Invest*. 2007;117:3198–3210.

8. Tirziu D, Chorianopoulos E, Moodie KL, Palac RT, Zhuang ZW, Tjwa M, Roncal C, Eriksson U, Fu Q, Elfenbein A, Hall AE, Carmeliet P, Moons L, Simons M. Myocardial hypertrophy in the absence of external stimuli is induced by angiogenesis in mice. *J Clin Invest*. 2007;117:3188–3197.

9. Moorjani N, Westaby S, Narula J, Catarino PA, Brittin R, Kemp TJ, Narula N, Sugden PH. Effects of left ventricular volume overload on mitochondrial and death-receptor-mediated apoptotic pathways in the transition to heart failure. *Am J Cardiol*. 2009;103:1261–1268.

10. Song H, Conte JV Jr, Foster AH, McLaughlin JS, Wei C. Increased p53 protein expression in human failing myocardium. *J Heart Lung Transplant*. 1999;18:744–749.

11. Condorelli G, Morisco C, Stassi G, Notte A, Farina F, Sgaramella G, de Rienzo A, Roncarati R, Trimarco B, Lembo G. Increased cardiomyocyte apoptosis and changes in proapoptotic and antiapoptotic genes bax and bcl-2 during left ventricular adaptations to chronic pressure overload in the rat. *Circulation*. 1999;99:3071–3078.

12. Hu P, Zhang D, Swenson L, Chakrabarti G, Abel ED, Litwin SE. Minimally invasive aortic banding in mice: effects of altered cardiomyocyte insulin signaling during pressure overload. *Am J Physiol Heart Circ Physiol*. 2003;285:H1261–H1269.

13. Liu X, Chua CC, Gao J, Chen Z, Landy CL, Hamdy R, Chua BH. Pifithrin-alpha protects against doxorubicin-induced apoptosis and acute cardiotoxicity in mice. *Am J Physiol Heart Circ Physiol*. 2004;286:H933–H939.

14. Shizukuda Y, Matoba S, Mian OY, Nguyen T, Hwang PM. Targeted disruption of p53 attenuates doxorubicin-induced cardiac toxicity in mice. *Mol Cell Biochem*. 2005;273:25–32.

15. Sano M, Minamino T, Toko H, Miyauchi H, Orimo M, Qin Y, Akazawa H, Tateno K, Kayama Y, Harada M, Shimizu I, Asahara T, Hamada H, Tomita S, Molkentin JD, Zou Y, Komuro I. p53-induced inhibition of Hif-1 causes cardiac dysfunction during pressure overload. *Nature*. 2007;446:444–448.

16. Menendez D, Inga A, Resnick MA. The expanding universe of p53 targets. *Nat Rev Cancer*. 2009;9:724–737.

17. Müller P, Kazakov A, Semenov A, Böhm M, Laufs U. Pressure-induced cardiac overload induces upregulation of endothelial and myocardial progenitor cells. *Cardiovasc Res*. 2008;77:151–159.

18. Marino S, Vooijs M, van Der GH, Jonkers J, Berns A. Induction of medulloblastomas in p53-null mutant mice by somatic inactivation of Rb in the external granular layer cells of the cerebellum. *Genes Dev*. 2000;14:994–1004.

19. Forde A, Constien R, Grone HJ, Hammerling G, Arnold B. Temporal Cre-mediated recombination exclusively in endothelial cells using Tie2 regulatory elements. *Genesis*. 2002;33:191–197.

20. Kossmann S, Hu H, Steven S, Schönfelder T, Fraccarollo D, Mikhed Y, Brähler M, Knorr M, Brandt M, Karbach SH, Becker C, Oelze M, Bauersachs J, Widder J, Münzel T, Daiber A, Wenzel P. Inflammatory monocytes determine endothelial nitric-oxide synthase uncoupling and nitro-oxidative stress induced by angiotensin II. *J Biol Chem*. 2014;289:27540–27550.

21. Toischer K, Rokita AG, Unsöld B, Zhu W, Kararigas G, Sosalla S, Reuter SP, Becker A, Teucher N, Seidler T, Grebe C, Preuss L, Gupta SN, Schmidt K, Lehnart SE, Krüger M, Linke WA, Backs J, Regitz-Zagrosek V, Schäfer K, Field LJ, Maier LS, Hasenfuss G. Differential cardiac remodeling in preload versus afterload. *Circulation*. 2010;122:993–1003.

22. Heida NM, Leifheit-Nestler M, Schroeter MR, Müller JP, Cheng IF, Henkel S, Limbourg A, Limbourg FP, Alves F, Quigley JP, Ruggeri ZM, Hasenfuss G, Konstantinides S, Schäfer K. Leptin enhances the potency of circulating angiogenic cells via src kinase and integrin (alpha)vbeta5: implications for angiogenesis in human obesity. *Arterioscler Thromb Vasc Biol*. 2010;30:200–206.

23. Wykoff CC, Beasley NJ, Watson PH, Turner KJ, Pastorek J, Sibtain A, Wilson GD, Turley H, Talks KL, Maxwell PH, Pugh CW, Ratcliffe PJ, Harris AL. Hypoxia-inducible expression of tumor-associated carbonic anhydrases. *Cancer Res*. 2000;60:7075–7083.

24. Vousden KH, Prives C. Blinded by the light: the growing complexity of p53. *Cell*. 2009;137:413–431.

25. Moorjani N, Catarino P, Trabzuni D, Saleh S, Moorji A, Dzimiri N, Al Mohanna F, Westaby S, Ahmad M. Upregulation of Bcl-2 proteins during the transition to pressure overload-induced heart failure. *Int J Cardiol*. 2007;116:27–33.

26. Leri A, Liu Y, Malhotra A, Stiegler P, Claudio PP, Giordano A, Kajstura J, Hintze TH, Anversa P. Pacing-induced heart failure in dogs enhances the expression of p53 and p53-dependent genes in ventricular myocytes. *Circulation*. 1998;97:194–203.

27. Naito AT, Okada S, Minamino T, Iwanaga K, Liu ML, Sumida T, Nomura S, Sahara N, Mizoroki T, Takashima A, Akazawa H, Nagai T, Shiojima I, Komuro I. Promotion of CHIP-mediated p53 degradation protects the heart from ischemic injury. *Circ Res*. 2010;106:1692–1702.

28. Zhu W, Soonpaa MH, Chen H, Shen W, Payne RM, Liechty EA, Caldwell RL, Shou W, Field LJ. Acute doxorubicin cardiotoxicity is associated with p53-induced inhibition of the mammalian target of rapamycin pathway. *Circulation*. 2009;119:99–106.

29. Feridooni T, Hotchkiss A, Remley-Carr S, Saga Y, Pasumarthi KB. Cardiomyocyte specific ablation of p53 is not sufficient to block doxorubicin induced cardiac fibrosis and associated cytoskeletal changes. *PLoS One*. 2011;6:e22801.

30. Osada M, Park HL, Park MJ, Liu JW, Wu G, Trink B, Sidransky D. A p53-type response element in the GDF15 promoter confers high specificity for p53 activation. *Biochem Biophys Res Commun*. 2007;354:913–918.

31. Anand IS, Kempf T, Rector TS, Tapken H, Allhoff T, Jantzen F, Kuskowski M, Cohn JN, Drexler H, Wollert KC. Serial measurement of growth-differentiation factor-15 in heart failure: relation to disease severity and prognosis in the Valsartan Heart Failure Trial. *Circulation*. 2010;122:1387–1395.

32. Jimenez B, Volpert OV, Crawford SE, Febbraio M, Silverstein RL, Bouck N. Signals leading to apoptosis-dependent inhibition of neovascularization by thrombospondin-1. *Nat Med*. 2000;6:41–48.

33. Spyridopoulos I, Brogi E, Kearney M, Sullivan AB, Cetrulo C, Isner JM, Losordo DW. Vascular endothelial growth factor inhibits endothelial cell apoptosis

induced by tumor necrosis factor-alpha: balance between growth and death signals. *J Mol Cell Cardiol*. 1997;29:1321–1330.

34. Riccioni T, Cirielli C, Wang X, Passaniti A, Capogrossi MC. Adenovirus-mediated wild-type p53 overexpression inhibits endothelial cell differentiation in vitro and angiogenesis in vivo. *Gene Ther*. 1998;5:747–754.

35. Teodoro JG, Parker AE, Zhu X, Green MR. p53-mediated inhibition of angiogenesis through up-regulation of a collagen prolyl hydroxylase. *Science*. 2006;313:968–971.

36. Assadian S, El Assaad W, Wang XQ, Gannon PO, Barres V, Latour M, Mes-Masson AM, Saad F, Sado Y, Dostie J, Teodoro JG. p53 inhibits angiogenesis by inducing the production of Arresten. *Cancer Res*. 2012;72:1270–1279.

37. Guan A, Gong H, Ye Y, Jia J, Zhang G, Li B, Yang C, Qian S, Sun A, Chen R, Ge J, Zou Y. Regulation of p53 by Jagged1 contributes to angiotensin II-induced impairment of myocardial angiogenesis. *PLoS One*. 2013;8:e76529.

38. Umar S, van der Laarse A. Nitric oxide and nitric oxide synthase isoforms in the normal, hypertrophic, and failing heart. *Mol Cell Biochem*. 2010;333:191–201.

39. Kodama T, Takehara T, Hikita H, Shimizu S, Shigekawa M, Tsunematsu H, Li W, Miyagi T, Hosui A, Tatsumi T, Ishida H, Kanto T, Hiramatsu N, Kubota S, Takigawa M, Tomimaru Y, Tomokuni A, Nagano H, Doki Y, Mori M, Hayashi N. Increases in p53 expression induce CTGF synthesis by mouse and human hepatocytes and result in liver fibrosis in mice. *J Clin Invest*. 2011;121:3343–3356.

40. Zeisberg EM, Tarnavski O, Zeisberg M, Dorfman AL, McMullen JR, Gustafsson E, Chandraker A, Yuan X, Pu WT, Roberts AB, Neilson EG, Sayegh MH, Izumo S, Kalluri R. Endothelial-to-mesenchymal transition contributes to cardiac fibrosis. *Nat Med*. 2007;13:952–961.

41. Moore-Morris T, Guimarães-Camboa N, Banerjee I, Zambon AC, Kisseleva T, Velayoudon A, Stallcup WB, Gu Y, Dalton ND, Cedenilla M, Gomez-Amaro R, Zhou B, Brenner DA, Peterson KL, Chen J, Evans SM. Resident fibroblast lineages mediate pressure overload-induced cardiac fibrosis. *J Clin Invest*. 2014;124:2921–2934.

42. Zeisberg M, Hanai J, Sugimoto H, Mammoto T, Charytan D, Strutz F, Kalluri R. BMP-7 counteracts TGF-beta1-induced epithelial-to-mesenchymal transition and reverses chronic renal injury. *Nat Med*. 2003;9:964–968.

43. Morimoto Y, Bando YK, Shigeta T, Monji A, Murohara T. Atorvastatin prevents ischemic limb loss in type 2 diabetes: role of p53. *J Atheroscler Thromb*. 2011;18:200–208.

44. Ramasubbu K, Estep J, White DL, Deswal A, Mann DL. Experimental and clinical basis for the use of statins in patients with ischemic and nonischemic cardiomyopathy. *J Am Coll Cardiol*. 2008;51:415–426.

45. Grillari J, Hohenwarter O, Grabherr RM, Katinger H. Subtractive hybridization of mRNA from early passage and senescent endothelial cells. *Exp Gerontol*. 2000;35:187–197.

46. Tyner SD, Venkatachalam S, Choi J, Jones S, Ghebranious N, Igelmann H, Lu X, Soron G, Cooper B, Brayton C, Park SH, Thompson T, Karsenty G, Bradley A, Donehower LA. p53 mutant mice that display early ageing-associated phenotypes. *Nature*. 2002;415:45–53.

47. Izumi N, Mizuguchi S, Inagaki Y, Saika S, Kawada N, Nakajima Y, Inoue K, Suehiro S, Friedman SL, Ikeda K. BMP-7 opposes TGF-beta1-mediated collagen induction in mouse pulmonary myofibroblasts through Id2. *Am J Physiol Lung Cell Mol Physiol*. 2006;290:L120–L126.

48. Okada H, Kikuta T, Kobayashi T, Inoue T, Kanno Y, Takigawa M, Sugaya T, Kopp JB, Suzuki H. Connective tissue growth factor expressed in tubular epithelium plays a pivotal role in renal fibrogenesis. *J Am Soc Nephrol*. 2005;16:133–143.

49. McMaken S, Exline MC, Mehta P, Piper M, Wang Y, Fischer SN, Newland CA, Schrader CA, Balser SR, Sarkar A, Baran CP, Marsh CB, Cook CH, Phillips GS, Ali NA. Thrombospondin-1 contributes to mortality in murine sepsis through effects on innate immunity. *PLoS One*. 2011;6:e19654.

50. Kodali R, Hajjou M, Berman AB, Bansal MB, Zhang S, Pan JJ, Schecter AD. Chemokines induce matrix metalloproteinase-2 through activation of epidermal growth factor receptor in arterial smooth muscle cells. *Cardiovasc Res*. 2006;69:706–715.

51. Bansal K, Kapoor N, Narayana Y, Puzo G, Gilleron M, Balaji KN. PIM2 Induced COX-2 and MMP-9 expression in macrophages requires PI3K and Notch1 signaling. *PLoS One*. 2009;4:e4911.

52. Mauro C, Leow SC, Anso E, Rocha S, Thotakura AK, Tornatore L, Moretti M, De Smaele E, Beg AA, Tergaonkar V, Chandel NS, Franzoso G. NF-kappaB controls energy homeostasis and metabolic adaptation by upregulating mitochondrial respiration. *Nat Cell Biol*. 2011;13:1272–1279.

53. Moon JO, Welch TP, Gonzalez FJ, Copple BL. Reduced liver fibrosis in hypoxia-inducible factor-1alpha-deficient mice. *Am J Physiol Gastrointest Liver Physiol*. 2009;296:G582–G592.

54. Wang JM, Singh C, Liu L, Irwin RW, Chen S, Chung EJ, Thompson RF, Brinton RD. Allopregnanolone reverses neurogenic and cognitive deficits in mouse model of Alzheimer's disease. *Proc Natl Acad Sci USA*. 2010;107:6498–6503.

55. Yates B, Zetterberg C, Rajeev V, Reiss M, Rittling SR. Promoter-independent regulation of vimentin expression in mammary epithelial cells by val(12)ras and TGFbeta. *Exp Cell Res*. 2007;313:3718–3728.

Endothelial p53 Deletion Improves Angiogenesis and Prevents Cardiac Fibrosis and Heart Failure Induced by Pressure Overload in Mice

Rajinikanth Gogiraju, Xingbo Xu, Magdalena L. Bochenek, Julia H. Steinbrecher, Stephan E. Lehnart, Philip Wenzel, Michael Kessel, Elisabeth M. Zeisberg, Matthias Dobbelstein and Katrin Schäfer

The online version of this article, along with updated information and services, is located on the
World Wide Web at:
http://jaha.ahajournals.org/content/4/2/e001770